Title: Sedimentological Analyses, Internal Stratigraphy and Sediment-hosted Detrital Iron and Radioactive Ore Mineral Potential of the Mesoarchean Siliciclastic Succession around Keonjhar, Singhbhum Craton, Odisha, India

Synopsis of the PhD thesis submitted for fulfilment of PhD Degree in Science (Geology) of the Presidency University, Kolkata

Saheli De
Department of Geology
Presidency University, Kolkata
2018

The pre submission synopsis (5000 words) is accepted and presentation was done accordingly. Recommended for final submission of the Thesis.

13/3/18

13/3/18

13.3.18

13/3/18 13/3/18

13/3/18

Title: Sedimentological Analyses, Internal Stratigraphy and Sediment-hosted Detrital Iron and Radioactive Ore Mineral Potential of the Mesoarchean Siliciclastic Succession around Keonjhar, Singhbhum Craton, Odisha, India

5000-word synopsis of the proposed PhD programme in Science (Geology) of the Presidency University

Saheli De

Submitted by: Saheli De
Department of Geology
Presidency University, Kolkata
2018

Registration Number: R-14RS15210051 of 2016

13.3.18

JOYDIP MUKHOPADHYAY, Ph D
Professor of Geology
Presidency University, Kolkata
INDIA

Title: Sedimentological Analyses, Internal Stratigraphy and Sediment-hosted Detrital Iron and Radioactive Ore Mineral Potential of the Mesoarchean Siliciclastic Succession around Keonjhar, Singhbhum Craton, Odisha, India

5000-word synopsis of the proposed PhD programme in Science (Geology) of the Presidency University

Submitted by: Saheli De
Department of Geology
Presidency University, Kolkata

1. INTRODUCTION

Precambrian sedimentary deposits are believed to record the history of development of Earth's early crustal composition, eustatic controls, nature of tectonics and early atmosphere (Taylor and McLennan 1985). Of particular interest is the nature of sediment depositional systems and combined effects of eustasy and tectonics on the development of basin-fills. Paleo-Eoarchean sedimentary records are mostly components of greenstone belts preserved in the granite-greenstone cores of early crust spread over different continents. The greenstone belts dominantly comprise of deep-marine graywacke-mudstone-volcaniclastics and BIF interbedded with metavolcanics. Such volcano-sedimentary stratigraphy dominated the rock record till the Mesoarchean. In contrast the shallow-marine/continental arenaceous sedimentary systems started appearing since later part of Mesoarchean, e.g., the Moodies Group and the Witwatersrand Supergroup in the Kaapvaal craton, South Africa, Bababudan Group in the Dharwar craton, India. These successions record the emergence of continental crust in significant proportion. Oldest such record comes from the ~3.2 Ga Moodies Group (Heubeck and Lowe 1994).

This PhD dissertation programme attempted to throw lights on the Mesoarchean arenite depositional system and nature of Mesoarchean upper crust from a collective study of internal stratigraphic development, interpretation of depositional settings and provenance analysis of the hitherto unclassified siliciclastic succession around Keonjhar Town in the Singhbhum craton, Odisha (Fig. 1) covering the study area under SOI Toposheets (73G/5, G/9, F/8, F/12). The dissertation has also explored the age of detrital iron ore deposits present in this succession and potential for radioactive placer mineral deposition.

2. OBJEVTIVES

Following objectives were proposed for the research programme:

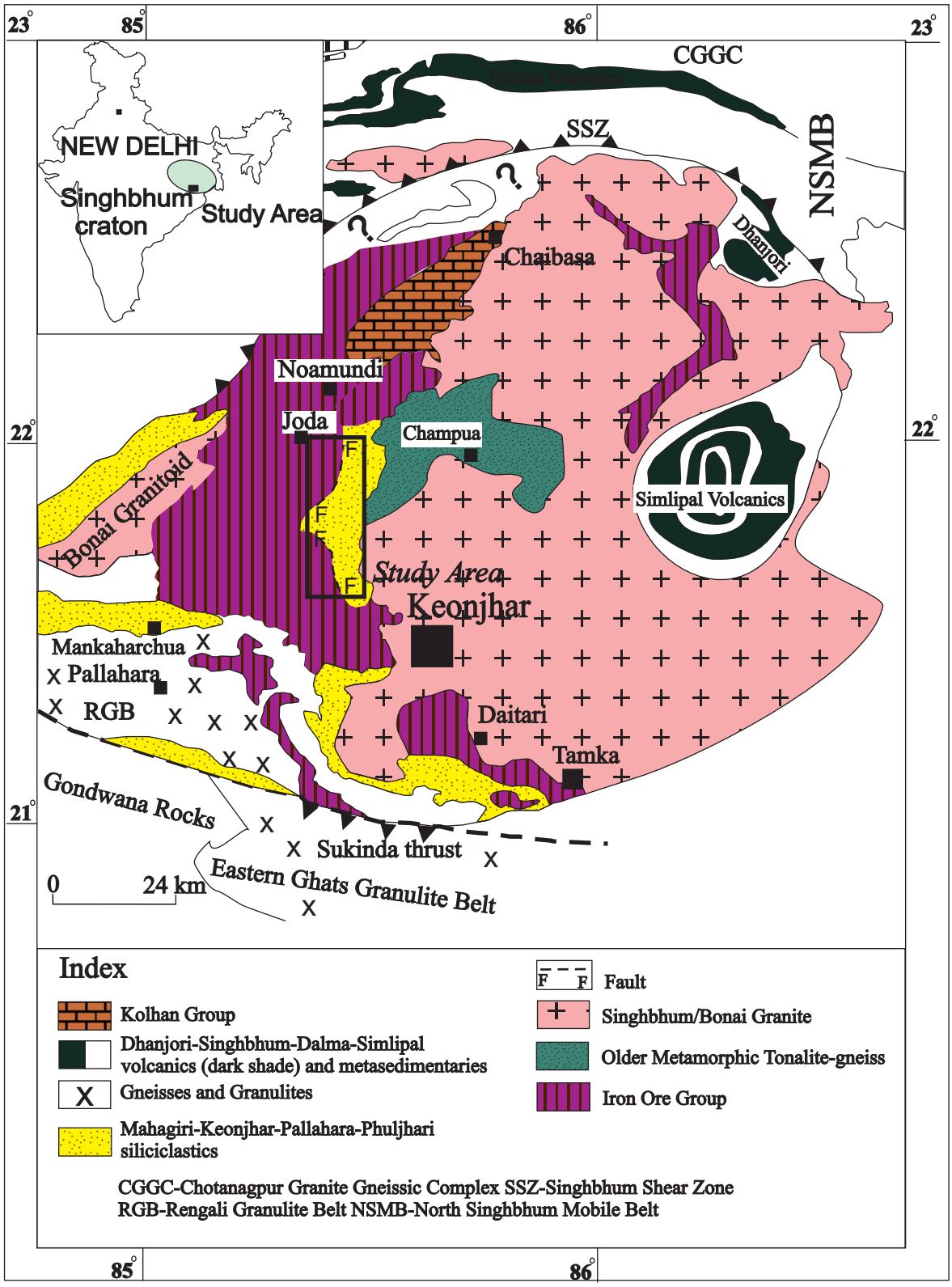

Figure. 1. Generalized geological map of the Singhbhum Craton (modified after Saha 1994).

1. To study in detail the depositional history of the siliciclastic succession around Keonjhar.
2. To attempt internal stratigraphy and U-Pb detrital zircon geochronology for constraining maximum depositional age.
3. To understand the composition and condition of the upper continental crust at Mesoarchean time from petrography and geochemistry of the siliciclastic succession.
4. To understand the differentiation of crust and mantle reservoir, Lu-Hf isotopic analysis in zircon has been used.
5. To study the detrital iron ore deposits and potential geochemical indicator for the U-Th paleoplacer in the succession.

3. METHODOLOGY

To get adequate information to fulfil the objectives of this research programme, the following methodologies have been adopted.

1. Internal stratigraphy of the hitherto unclassified siliciclastic succession in the proposed area has been worked out.
2. Sedimentary facies analysis was undertaken to reconstruct depositional environment.
3. To understand the composition and geodynamic condition of the upper continental crust at Mesoarchean time petrography from microscope, scanning electron microscope with Cathodoluminescence (SEM-CL) and the bulk geochemical analysis have been done with the help of X-ray Fluroscence (XRF) and ICPMS analysis.
4. To assess the sedimentological and stratigraphic controls on the possibility of enrichment of the U-Th paleoplacer in the siliciclastic succession geochemical proxies have been studied.
5. To understand the internal stratigraphy and U-Pb detrital zircon geochronology for constraining maximum depositional age for this siliciclastic succession by using LA-ICPMS methodology.
6. To understand the crust-mantle proportion at early Archean time and geodynamics condition for formation of granite at this time MC-ICP-MS Lu-Hf isotopic technique has been carried out.

4. INTERNAL STRATIGRAPHY

The Singhbhum craton in eastern India is constituted by a granite-greenstone core, Mesoarchean to Mesoproterozoic supracrustal cover sequences and peripheral mobile belts along northern and southern margins (Fig. 1) (Saha 1994). The granite-greenstone core records granite emplacement at three phases ranging in age between 3.4 Ga to 3.1 Ga (the Singhbum Granite Phases I, II and III). The granitoids are essentially Archean TTG components, oldest of which is referred to as Older Metamorphic Tonalite Gneiss (OMTG) and which is considered equivalent to the Singhbhum Granite phase I (3.44 Ga) (Mukhopadhyay 2001; Misra 2006). The greenstones with thick metabasalt-BIF-shale/volcaniclastics either occur as narrow linear enclaves of synformal keels in the western, eastern and southern peripheries of the granitoid core traditionally known as the Iron Ore Group (IOG) or as numerous small metasedimentary-metavolcanic enclaves of relatively higher metamorphic grade within the granitoids, collectively referred to as Older Metamorphic Group (OMG). The three prominent synformal keels with thick BIF-hosted iron ore deposits in each are referred to as Eastern, Western and Southern Iron Ore Group (IOG) (Saha 1994, Beukes et al. 2008). U-Pb zircon ages from the metalavas from southern IOG suggest a Paleoarchean (3.51 Ga) age (Mukhopadhyay et al. 2008) for the oldest greenstone component in the craton so far. Subsequent stratigraphic development is recorded in the siliciclastics dominated successions of the Dhanjori Group in the northern (ranging in age from >2.8 Ga to 2.2 Ga (Mazumder et al. 2012; Acharyya et al. 2010) and Mahagiri Quartzite and the siliciclastic succession around Keonjhar and Mankaharchua (Mukhopadhyay et al. 2015) along the southern and western peripheries of the craton.

The siliciclastic succession under study is ~715 m thick and unconformably overlies the Singhbhum Granite (3.1 Ga to 3.4 Ga) and the Western IOG around Keonjhar Town (Fig.1) with locally developed Keonjhar *Paleosol* along the unconformity (Mukhopadhyay et al. 2014). The succession is dominated by low-dipping mature sandstone with conglomerate interbeds in its lower parts.

The Keonjhar siliciclastics are essentially mature arenitic sandstones that can be mapped in 1:50000 scale. Based on criteria such as distinctive lithology and mappability I proposed here a formal lithostratigraphic status of the rank of a formation and named the unit as Keonjhar Quartzite (Fig. 2). Keonjhar Quartzite includes further two distinctive lithologies that are not mappable in practicable scale. The lower part of the succession includes conglomerate and pebbly sandstone interbedded with coarse-grained sandstone. The conglomerate-pebble sandstone-coarser sandstone association has been assigned here

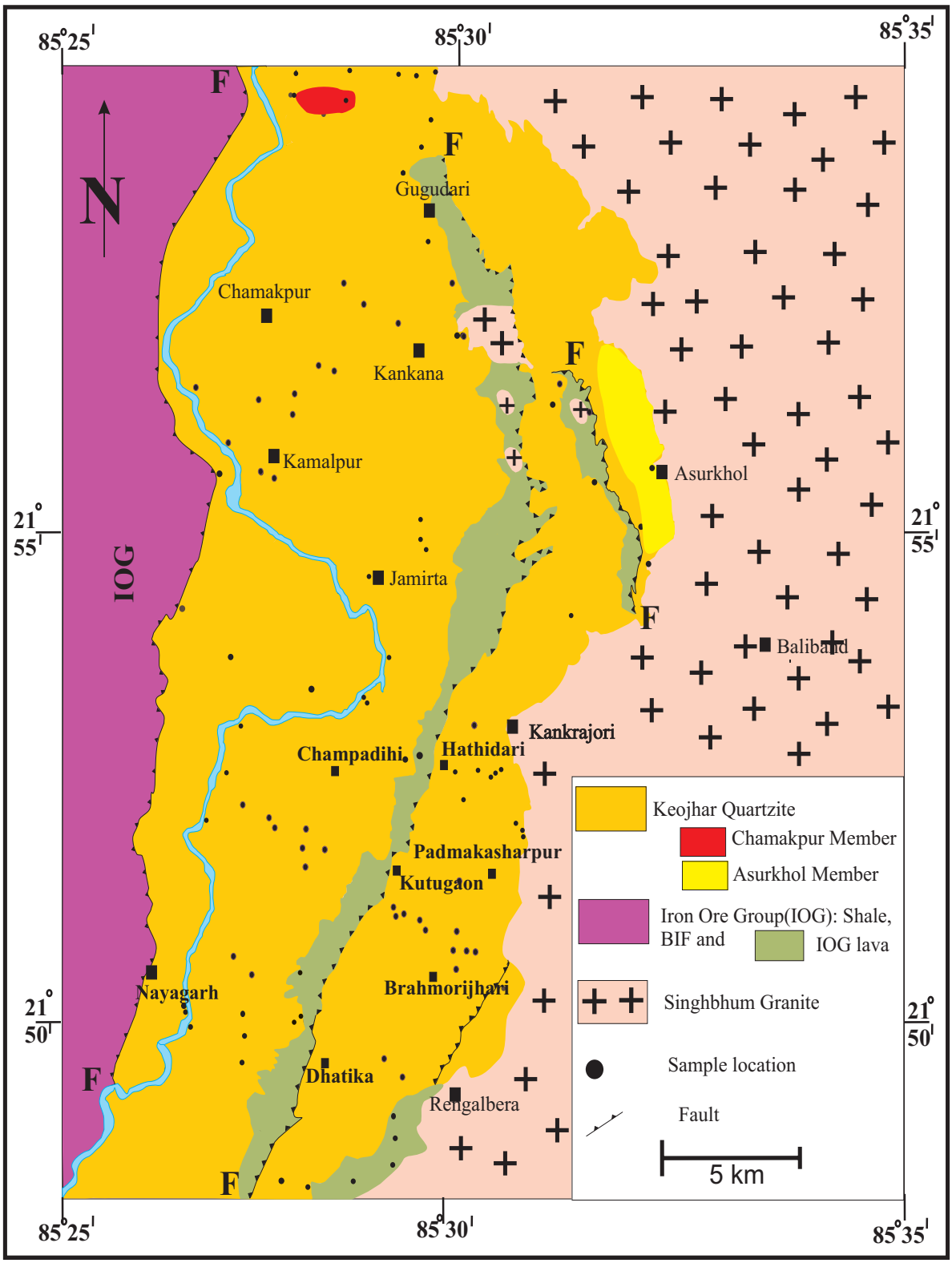

Figure. 2. Geological map of the Keonjhar Quartzite, north of Keonjhar Town

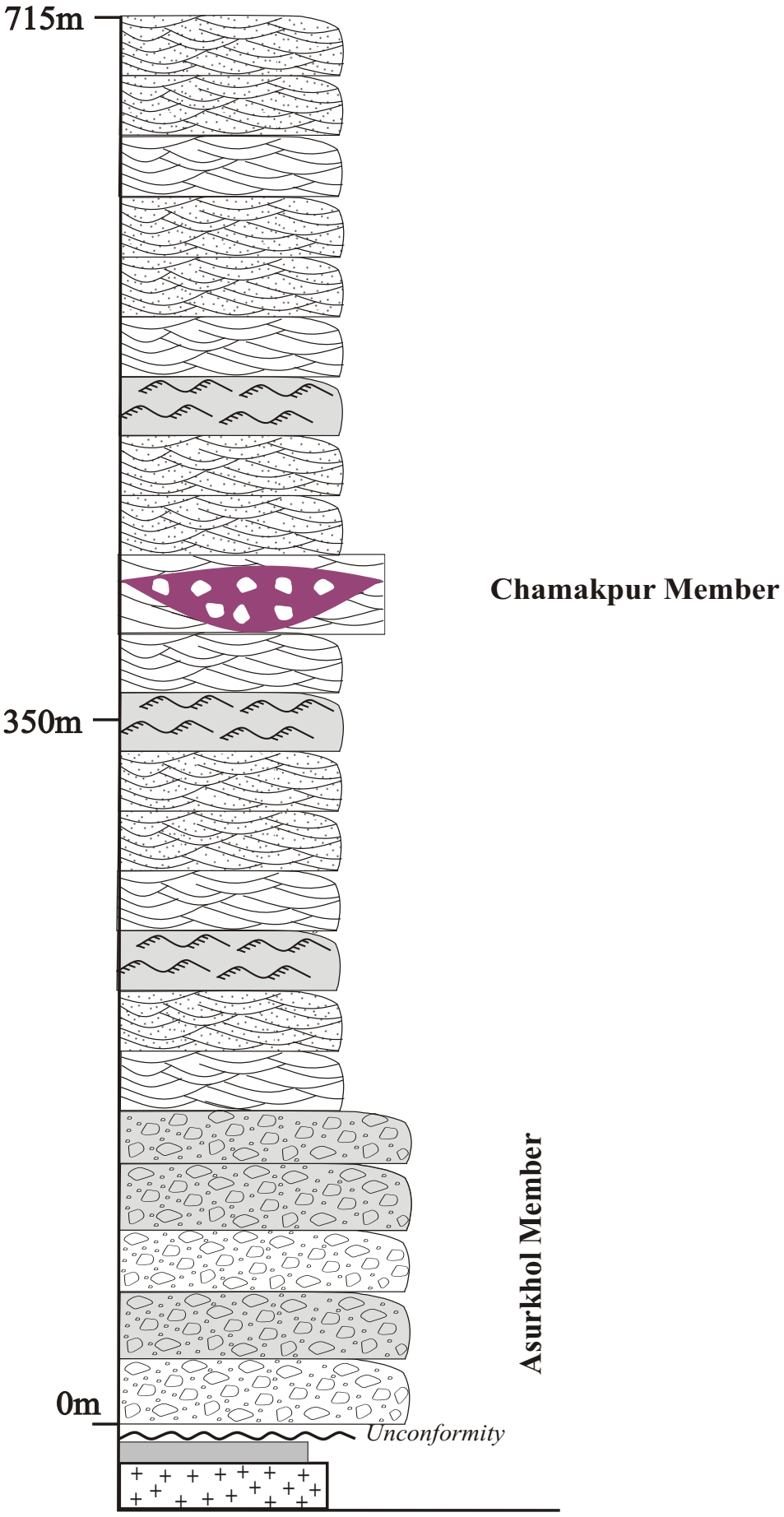

Figure. 3. Composite stratigraphic succession of the Keonjhar Quartzite. Note: two members classified within this formation: Asurkhol Member and Chamakpur Member

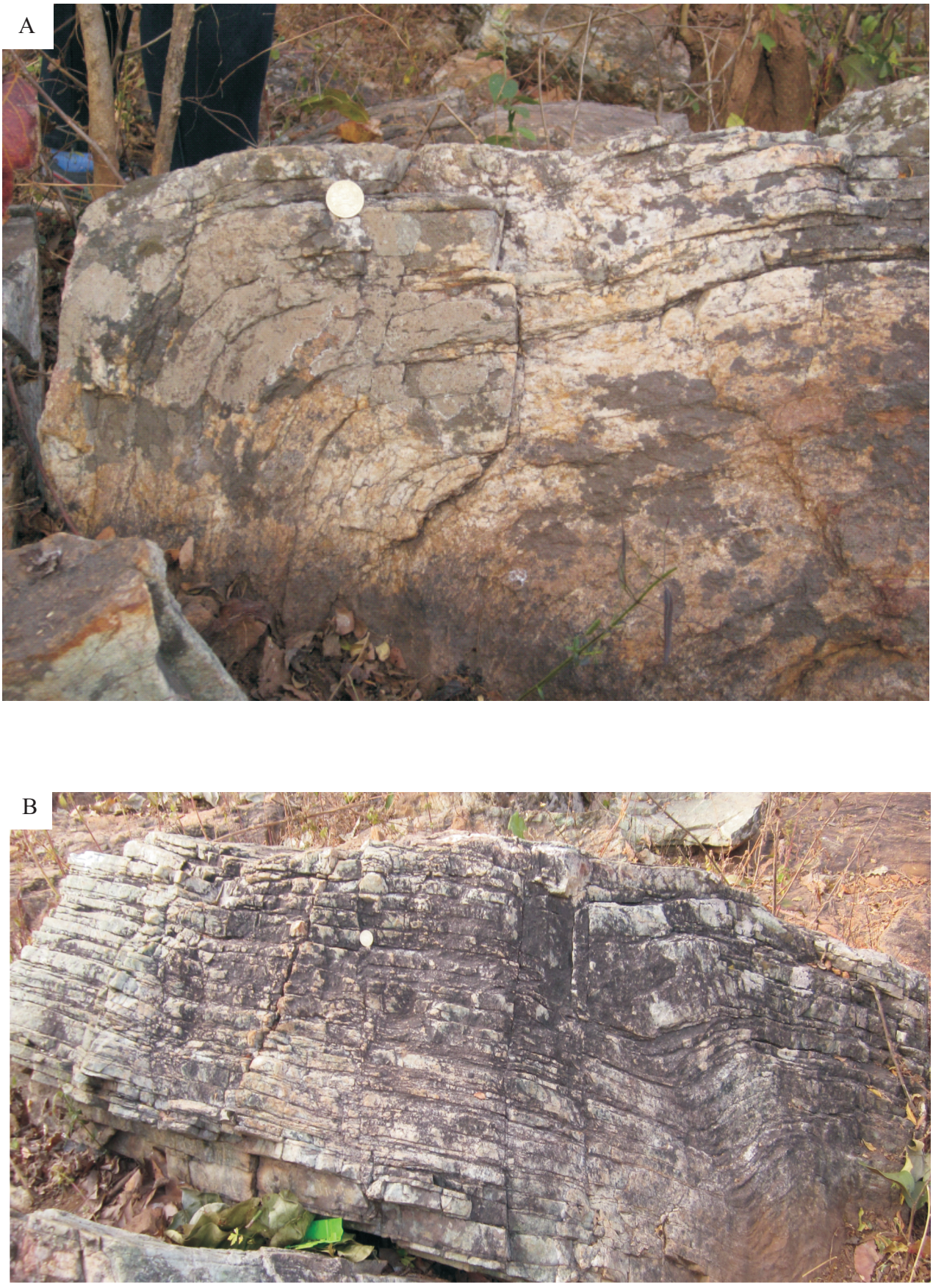

Figure. 4. Field photographs of megascopic deformation structures close to major faults in Keonjhar Quartzite: (A) locally developed asymmetric fold and (B) strong fracture cleavage

status of a member. The association is 25 m thick and is best preserved in the Asurkhol hill section (Lat. 21°55′54.9″ Long. 85°32′13.0″) and is named here as Asurkhol Member (Fig. 3). The other distinctive lithology is a pocket of iron ore-BIF clast-bearing conglomerate. The iron ore clast-bearing conglomerates occur as amalgamated mass-flow beds in a zone of about 40 m thickness and about 150 m width with mature arenite near the upper part of the Keonjhar Quartzite. The most prominent body (Fig. 3) is exposed in the hills of Chamakpur village (Lat. 21°59′32.8″ Long. 85°28′27.1″). The laterally restricted mode of occurrence of the conglomerate renders them a form of a lentil and a member status is proposed here. The lentil is named here as Chamakpur Member (Fig. 2).

The beds in the Keonjhar Quartzite are gently westerly dipping with in general dip amount not exceeding 15 degrees. The Keonjhar Quartzite in the study area unconformably overlies the Singhbhum Granite or IOG metabasic lava. The outcrop pattern (Fig. 2) reveals that the basement has been repeated in three major fault slices. The faults are in general N-S oriented and are sub parallel to the general strike of the beds. Locally developed asymmetric/symmetric folds (Fig. 4A and Fig. 4B), strong fracture cleavage and repetition of stratigraphy confirm the fault slices.

Table: 1. The proposed lithostratigraphic classification of Keonjhar Quartzite, Singhbhum craton, Odisha.

Keonjhar Quartzite Formation	Trough cross-stratified medium-to-coarse grained mature sandstone, pebbly sandstone, conglomerate	Chamakpur Member	Lentil shaped iron ore clast-bearing conglomerate
		Asurkhol Member	Trough cross stratified coarse grain mature sandstone. Matrix-supported conglomerate and Clast-supported conglomerate
----------*unconformity*----------			
Singhbhum Granite phase I- III-OMTG with IOG-OMG enclaves			

5. FACIES ANALYSIS OF KEONJHAR QUARTZITE

Based on lithology, grain size, grain-support and sedimentary structures the Keonjhar Quartzite has been classified into following facies and summarized in Table: 2 (Fig. 5 A-F and Fig. 6 A-D).

Table: 2. Salient characteristics of lithofacies in the Keonjhar Quartzite.

Lithofacies Type	Interpretation
a) Matrix-supported cobble-pebble conglomerate facies (F1) (Fig: 5A): Matrix-supported nongraded, massive.	Matrix indicates a cohesive debris flow (Nemec and Steel 1984), absence of grading also supports debris flow. A base-of-slope deposit at proximal subaerial fan (cf. Bluck 1967).
b) Clast-supported cobble-pebble conglomerate facies (F2) (Fig: 5B): Clast-supported nongraded, massive, sheet-like geometry.	Deposited from cohesionless debris flow, poorly sorted nature, less matrix component, lack of gradation, wavy geometry at the top of the bounding surface and sheet-like geometry. Deposited from steeper slopes, subaerial (Collinson et al. 1989; Tanner and Hubert 1991), wave reworked locally.
c) Wavy bedded pebbly sandstone (F3) (Fig: 5C): Poorly sorted, sandstone with dispersed pebbles, internally trough/planar stratified, wavy upper bounding surface.	Deposited from high-energy bedload transport. Wavy upper bounding surface suggests reworking by waves after deposition.
d) Fine-chip pebble conglomerate (F4) (Fig: 5D): Thin bedded, sheet-like, pebbly conglomerate internally massive, and wavy upper bounding surface.	The fine-chip pebble conglomerate internally massive is likely to be a product of cohesionless high-density flow. Wavy top is the indication of deposition in shallow water above wave base environment during storm events.
e) Coarse massive sandstone with pebble float facies (F5) (Fig: 5E): Coarse sand size grade, poor sorting, dispersed pebbles, sheet-like geometry.	Coarse and massive in nature, chaotic float within this facies is the product of sediment gravity flow/high-density sandy debris flow (Nemec and Steel 1984) and are likely to be products of storm-surge deposits from subaerial fan head to shallow shelf.
f) Pebble lag facies (F6) (Fig: 5F): Pebble thin, veneers of pebble beds between two wavy bedded sandstones, well rounded and well sorted grains, laterally extensive.	Pebble lag facies are interbedded with the wavy bedded mature quartz arenite facies, rounded to well-rounded pebble support recycling, the coarser lag deposit is formed from erosion of the alluvial deposits along the beach scarp and fair weather winnowing fine-grained fraction by wave action (cf. Orton and Reading 1993).
g) Trough cross-stratified medium-grained facies (F7) (Fig: 6A): Medium-to-thick-bedded arenite with sets of trough cross strata.	High-energy bedload deposits. Sets constitute cosets in a subaerial braid bar.
h) Plane-laminated medium-grained mature sandstone facies (F8) (Fig: 6B): Medium grained, well sorted, plane-laminated sandstone with low angle truncation between.	Plane lamination within the medium grain sandstone suggests high energy conditions were marked by the plane laminated sandstone layer (Miall 1978). Horizontally, bedded and planar low-angled cross-stratified sandstones reflect the foreshore-beach traction current (Mueller and Corcoran, 1998) under upper flow regime (Eriksso 1978; Fedo and Cooper, 1990).
i) Plane-to-wavy bedded cross-stratified medium-to-fine-grained sandstone facies (F9) (Fig: 6C and Fig. 6D):	Plane laminated-to-wavy bedded medium-grained sandstone facies reflect medium-to-high energy condition of deposition within wave base.

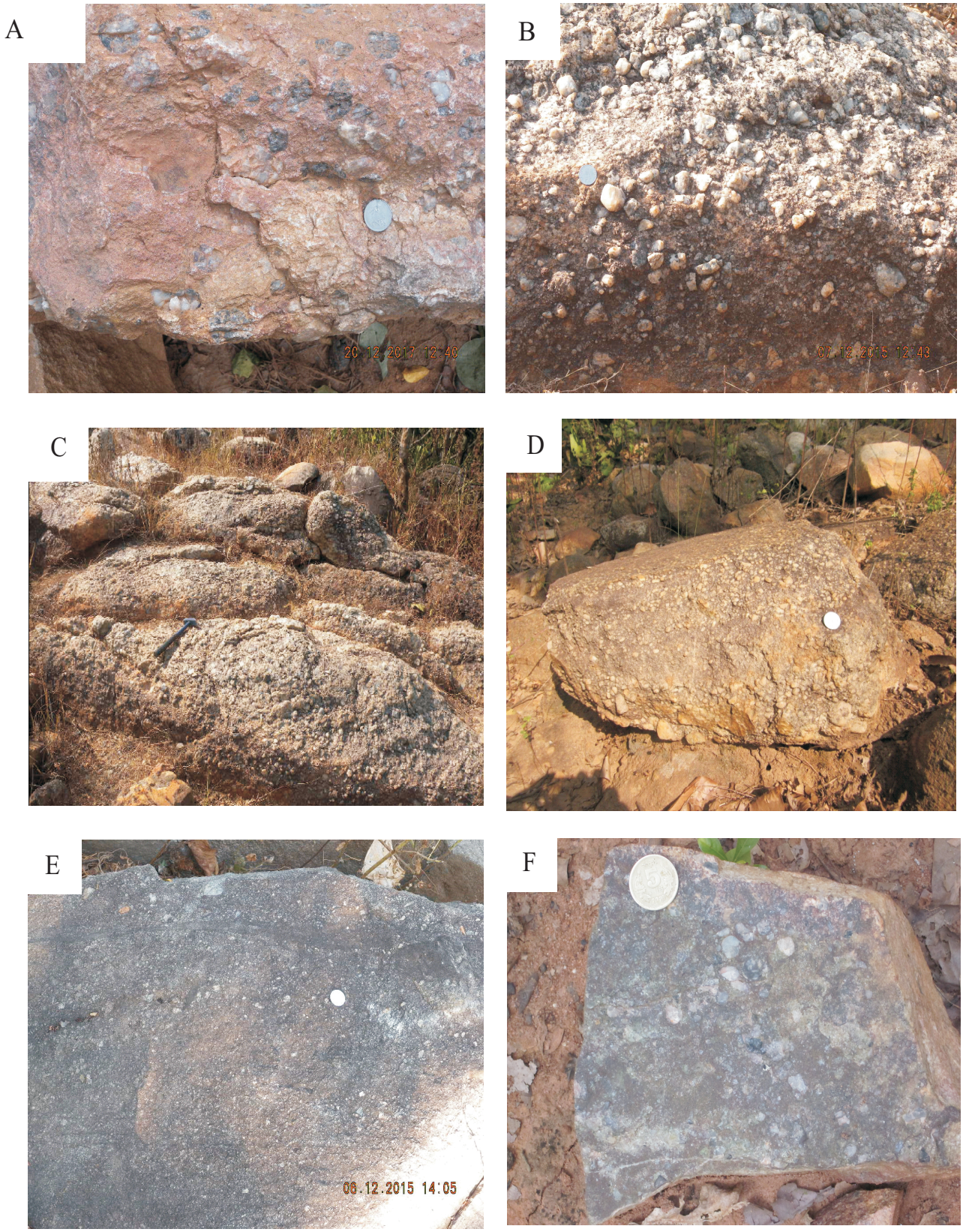

Figure. 5. Field photographs of different types of facies from Keonjhar Quartzite:(A) Matrix-supported cobble-to-pebble conglomerate facies (F1), (B) Clast-supported cobble-to-pebble conglomerate facies (F2), (C) Wavy bedded pebbly sandstone (F3), (D) Fine-chip pebble conglomerate (F4), (E) Coarse massive sandstone with pebble float facies (F5) and (F) Pebble lag facies (F6).

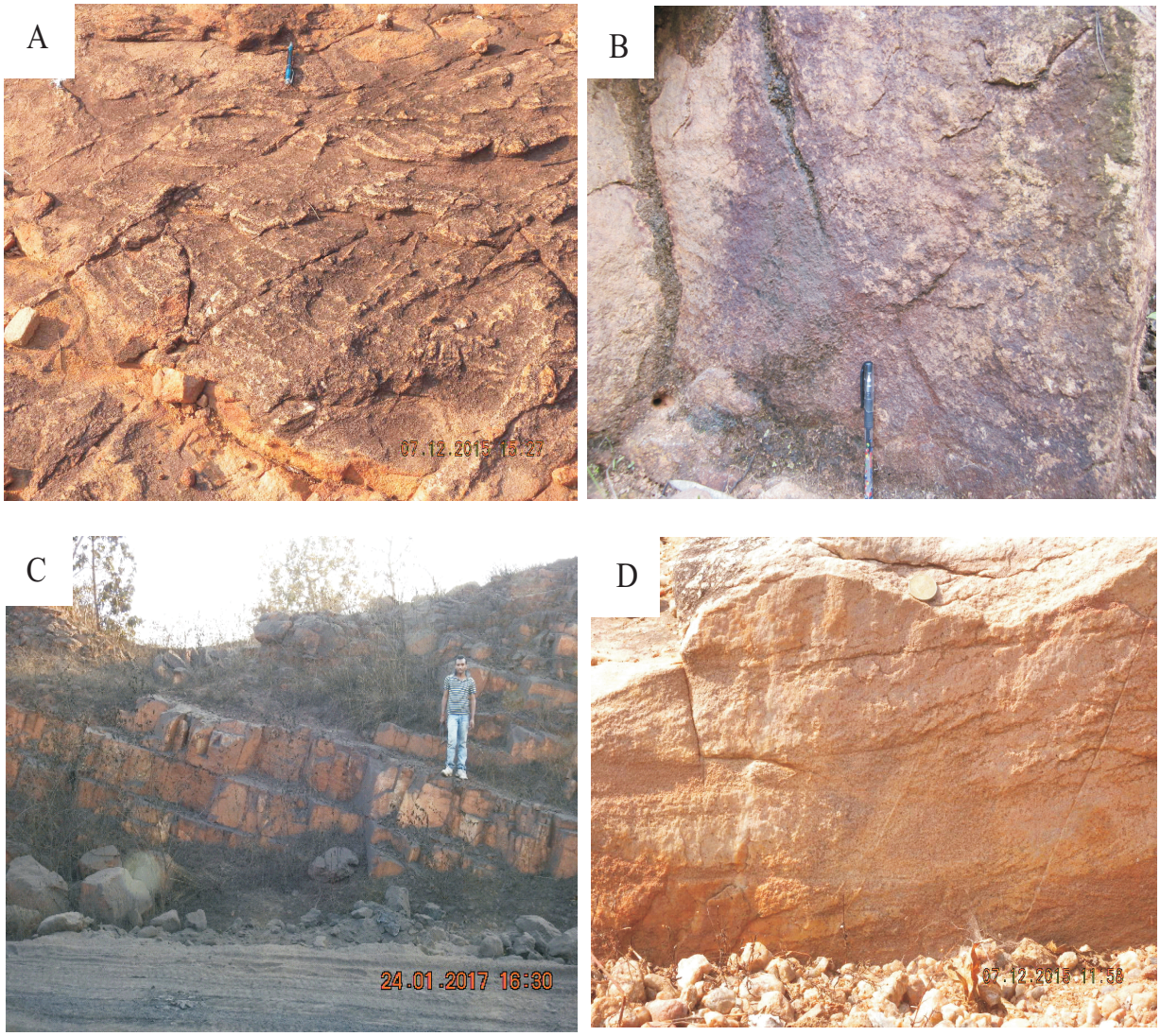

Figure. 6. Field photographs of different types of facies from Keonjhar Quartzite: .(A) Trough cross-stratified medium-grained sandstone facies (F7), (B) Plane-laminated medium-grained mature sandstone facies (F8) , (C) Wavy bedded medium-grained sandstone facies (F9), (D) Internal bedsets of cross-strata in wavy bedded structure of medium grained sandstone facies (F9).

The facies described above may be grouped into following four facies associations (Fig. 7).

A. *Matrix-supported Conglomerate dominated lithofacies association (FA1)*

This facies association includes F-1, F-2, and F-7 lithofacies of primarily slope-related subaerial mass-flow (cohesive). This cohesive debris flow deposits represent the most proximal part of a subaerial fan setting. The subaerial mass flow deposits accumulate in incised valleys within feeder channels of the alluvial fan slope-to base of slope. This facies association is very well exposed at the lower part as Asurkhol Member. This facies association attains a maximum thickness of about 25 meters.

B. *Clast-supported conglomerate dominated lithofacies association (FA2)*

This facies association includes F-2, F-7, F-4, and F-1 lithofacies. This facies association is also dominated by mass-flow (cohesionless) and is likely to represent medial part of a suabaerial fan and braid plain depositional setting. This facies association is likely to represent alluvial fan and braided plain depositional setting in fan delta type environment where coarser beds from braid plains or base of the fan slope extends subaqueous into shallow shelf. This facies association constitutes maximum thickness 12 meters in the Asurkhol Member in fault slices west of FA-1.

C. *Coarse-to-medium-grained pebbly sandstone dominated lithofacies association (FA3)*

This facies association represents F-3, F-4, F-5, and F-7 lithofacies. This facies association is dominated by wave-reworked pebbly sandstone, chip conglomerate, sandstone with floating pebbles, with interbeds of trough cross-stratified sandstone. Deposits from coarse-grained debris-flow and sandy debris flow with interbeded trough-cross-stratified cosets of sand bars indicate a transition from slope-derived mass-flow and braid plain fluvial deposits similar to FA-2 extending into shallow marine wave reworking zone of foreshore.The evidence of such wave-reworking suggests that braidplain is likely to be the subaqueos parts of a fandelta\braiddelta.

D. *Thick-bedded trough to planar cross-stratifiedmature sandstone dominated lithofacies association (FA4)*

This facies association represents F-9, F-8, and F-6 lithofacies. Wavy bedded compound cross strata with plane-laminated mature sandstone indicate deposition in wave-dominated shelf setting. The absence of coarse sandstone with pebbles indicates a wave-dominated shallow marine outer shelf deposit depositional environment.

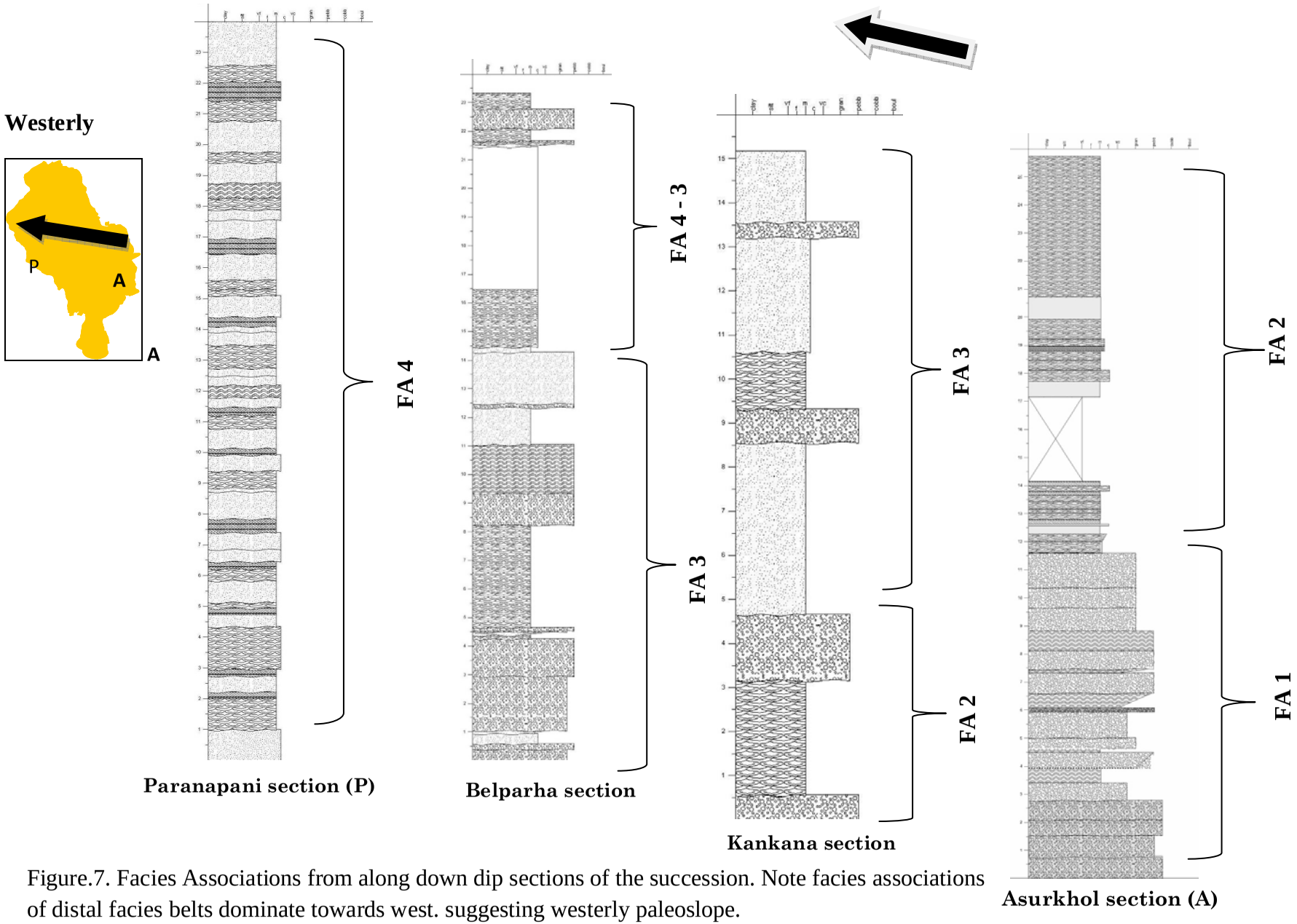

Figure.7. Facies Associations from along down dip sections of the succession. Note facies associations of distal facies belts dominate towards west. suggesting westerly paleoslope.

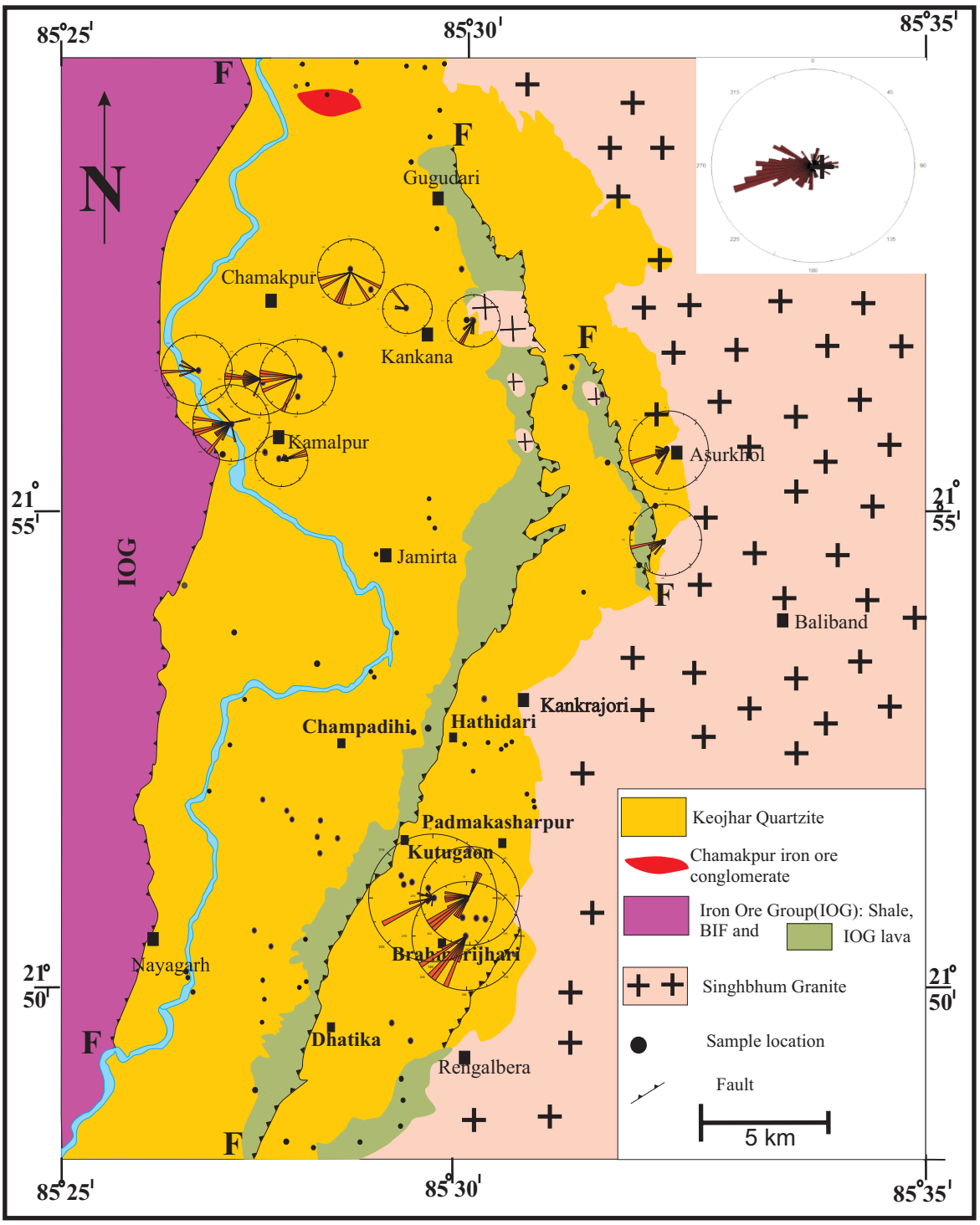

Figure. 8. Paleocurrent distribution pattern from trough cross-stratified sandstones of the Keonjhar Quartzite, Singhbhum Craton, Odisha.

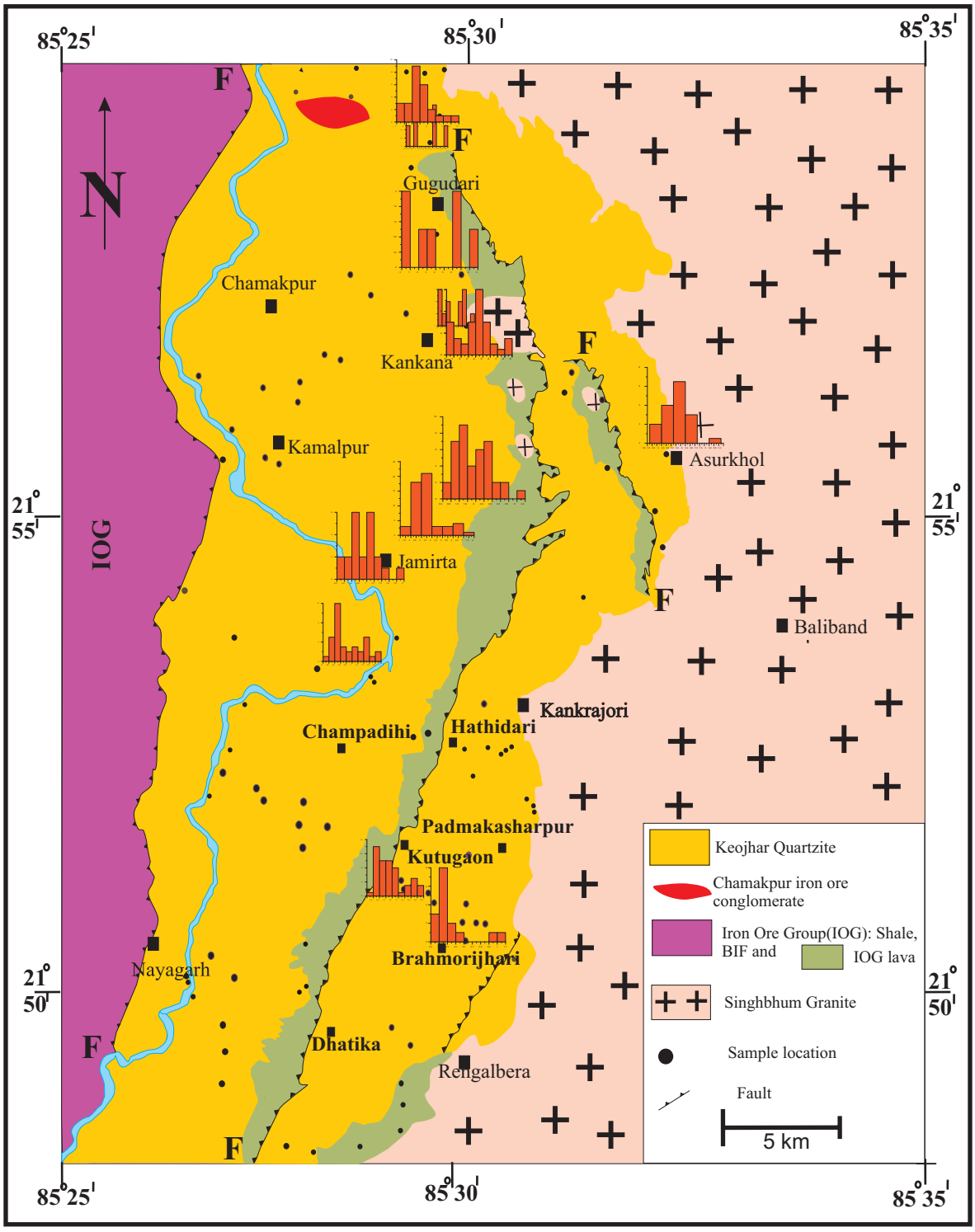

Figure. 9. Grain-size distribution histogram pattern conglomerate facies (ten largest clasts measured from each bed). Note. enrichment of smaller fraction towards west.

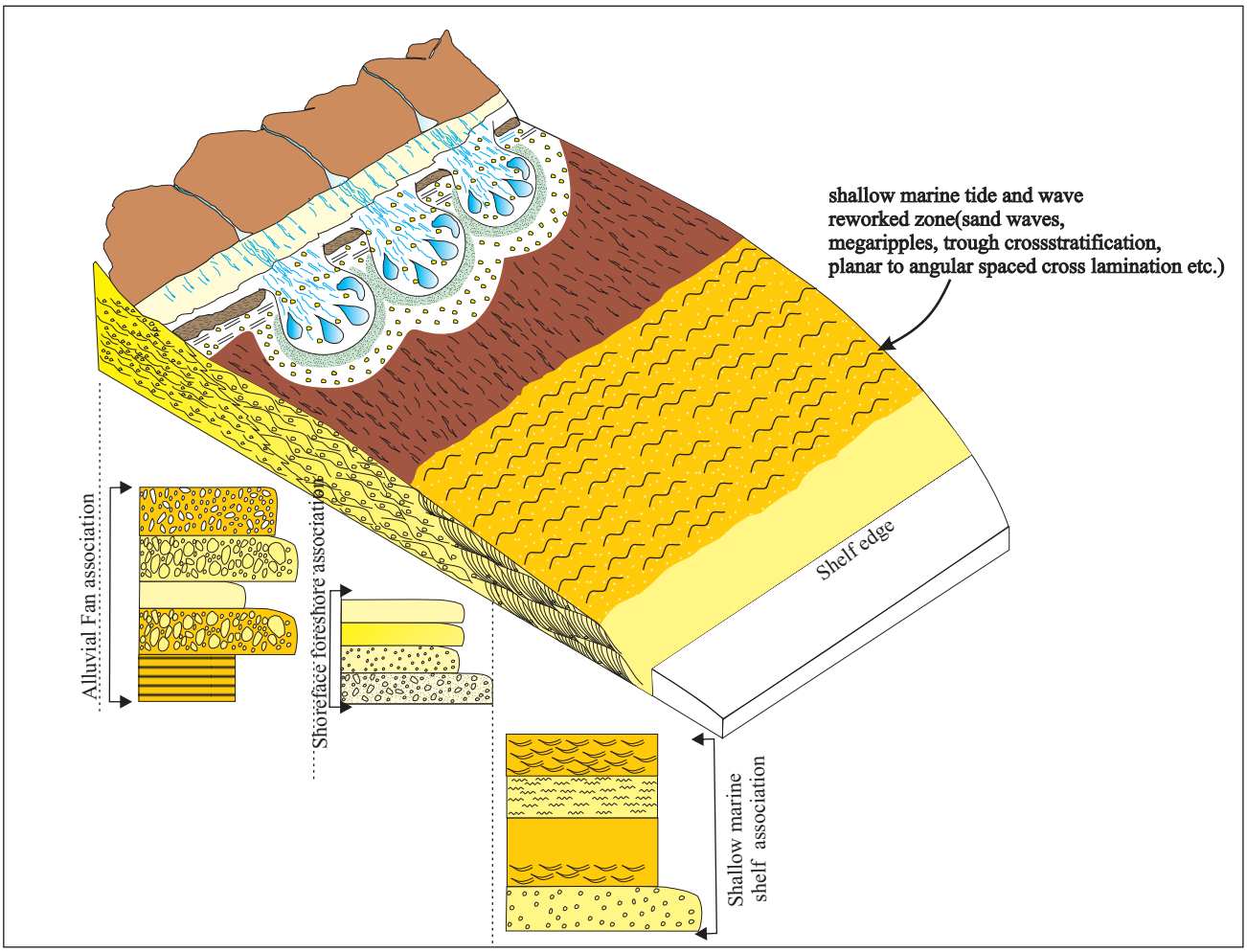

Figure. 10. Schematic depositional model for the Keonjhar Quartzite

Paleocurrent: Paleocurrent distribution is mainly dominant in unimodal or multimodal distribution with a preferred WSW-ly (255º) direction. Unimodal data dominated in the Harijori, Kankana and Gugudari area with the preferred dominant direction varies 245º to 255º (Fig. 8). Locally, bipolar distrbution with a weak SE-ly direction has been observed. Dominantly unidirectional current in wavy bedded sandstone with evidences of bipolarity indicates that the downlapping strata of wavy bedded sandstones that are the most dominant lithology in the Keonjhar Quartzite have been influenced by strong WSW-ly directed ebb tidal current (cf. Witts et al., 2012). Multidirectional paleocurrent observed in someplaces is likely to be storm and longshore drift signatures within the shallow marine shelf deposits (Gray and Benton, 1982)

Depositional Setting: The generalized lithofacies associations show progression of conglomerate-pebbly sandstone- to mature medium-grained sandstone upward-fining cycle. The ~715 m thick upward-fining successions in the Keonjhar Quartzite displays rapid changes of the high-energy, alluvial-fluvial, to wave-and-tide influenced shallow marine shelf deposits. The facies association (FA1-FA2-FA3-FA4) stacking pattern suggests such changes from alluvial fan to shallow marine shelf depositional environment. An alluvial fan-braid plain (fan delta) to shallow-marine shelf depositional setting is conceived here based on facies analyses (Fig.9 and Fig. 10).

Sequence Development

The succession is interpreted here in terms of a 'sequence' consisting of lowstand systems tract (LST), transgressive systems tract (TST) and highstand systems tract (HST) (Fig. 11). The Asurkhol Member with mass-flow conglomerate-dominated proximal-midfan depositional setting is considered here to constitute the LST. The base of the LST is marked by the major unconformity and many localized channelized conglomerates are likely to be incised valley fills (IVF) from the early Falling Stage Systems Tract (FSST). The interbedded conglomerate – sandstone association of the FA-2 forms the upper part of the LST which is characterized by repeated progradational sandstone-conglomerate interbeds in a progradation normal regressive phase of the base level during terminal LST. The appearance of well sorted, clast-supported pebbly conglomerate, fine chip conglomerates and pebble lags in FA-3 with sandstone beds marks the onset of the TST. Lowest of the pebble lags or a thin bed of laterally persistent chip conglomerate mark the transgressive lag surface, FA-4 with wavy bedded sandstone and pebble lag is likely to represent the TST phase. The uppermost part of the succession

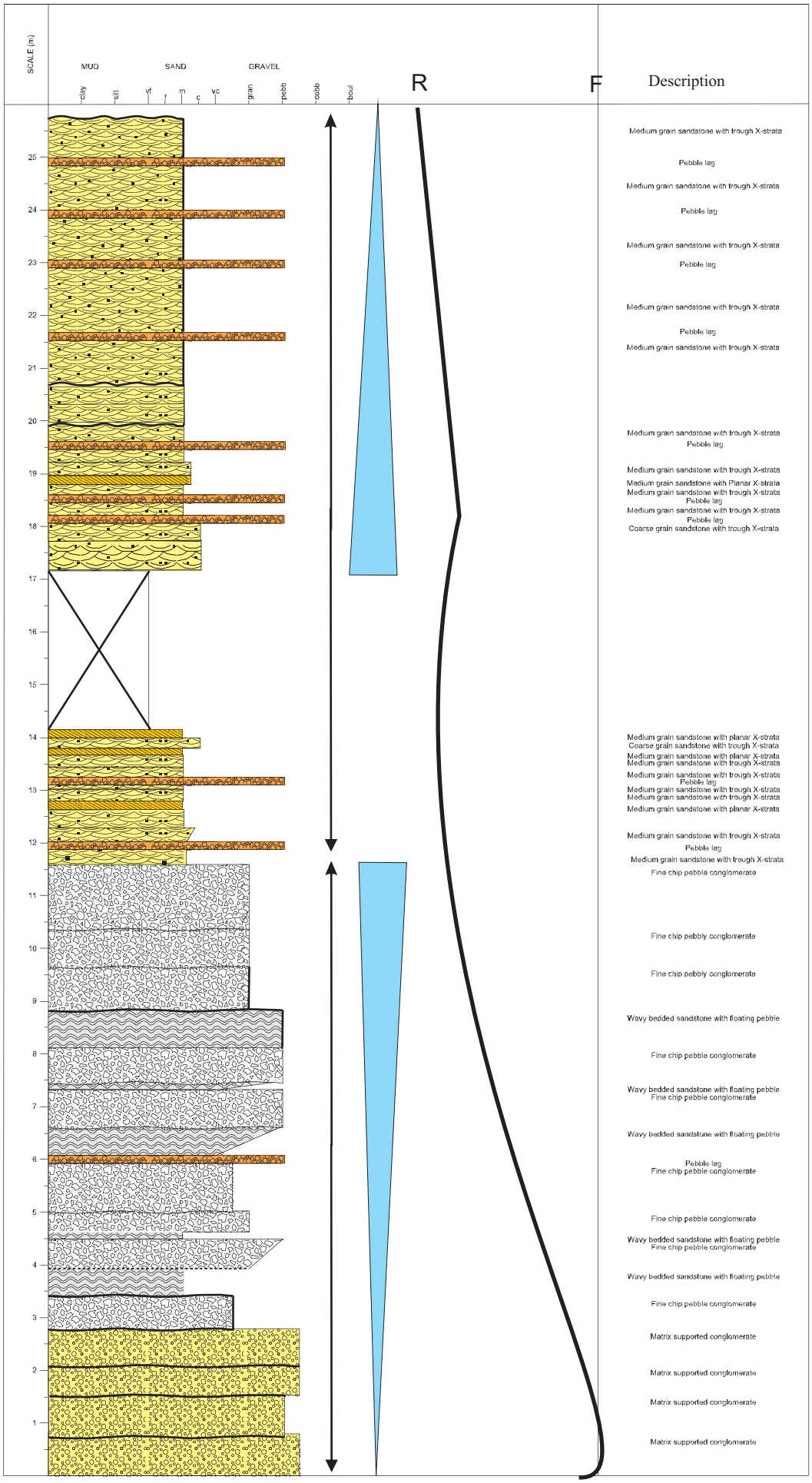

Figure. 11. Depositional sequence and systems tract from Keonjhar Quartzite.

dominated by mature wavy bedded sandstone of subequal thickness is likely to indicate aggradational stacking pattern in the later phase of TST or early part of the HST (Fig. 11).

6. PETROGRAPHY AND SEM-CL OF THE KEONJHAR QUARTZITE: IMPLICATION FOR PROVENANCE

Petrographic studies of the quartzarenite collected from Keonjhar area reveals that, they are generally angular to sub-angular in nature. Framework grain is mainly comprised of quartz grains. Grain contacts are generally straight, concavo convex and sutured in nature with neighboring quartz grains (Fig. 12). Modal analysis of the sandstones was done using a combined petrographic-chemical technique (Dickinson 1985 and Cox and Lowe methods, 1996) that takes into account the contribution from framework as well as from major oxide chemistry of secondary matrix. Modal petrographic analyses were plotted in three triangular tectonic discrimination diagrams, namely, Q_t-*F-L,* Q_m-*F-*L_t *and* Q_m-*P-K* (Dickinson 1985). Samples fall within the range of craton interior to recycled orogen and in a stable shelf setting (Fig. 13).

Scanning electron microscope cathodoluminescence (SEM-CL) analysis framework grains were carried out to classify the source rock types of the quartz framework grains. SEM-CL fabric analysis of the quartz grains identifies five types of quartz: plutonic quartz with healed fractures and mottled CL, medium-grade metamorphic quartz with mottled CL intensity, low-grade metamorphic quartz with low or patchy luminescence, quartz with internal brittle fractures and bright luminescent quartz (after Krinsley and Tovey 1978; Seyedolali et al. 1997; Fig. 14 and Fig. 15).

The modal framework compositions of the arenites from the Keonjhar Quartzite suggest *recycled orogen to craton interior provenance*. The *tectonic discrimination diagrams* also indicate the supermature nature of the sandstone derived from the interior of a stable continental craton. SEM (CL) analyses further suggest plutonic igneous dominated source terrain.

7. GEOCHEMICAL STUDIES OF THE KEONJHAR QUARTZITE: IMPLICATION IN PROVENANCE

Tectonic discrimination from major element composition: (e.g., TiO_2-Fe_2O_3+*MgO and* Al_2O_3/SiO_2 *Vs* (Fe_2O_3+*MgO),* K_2O/Na_2O-SiO_2 *and* SiO_2/Al_2O_3 –K_2O/Na_2O *after* Bhatia 1983;

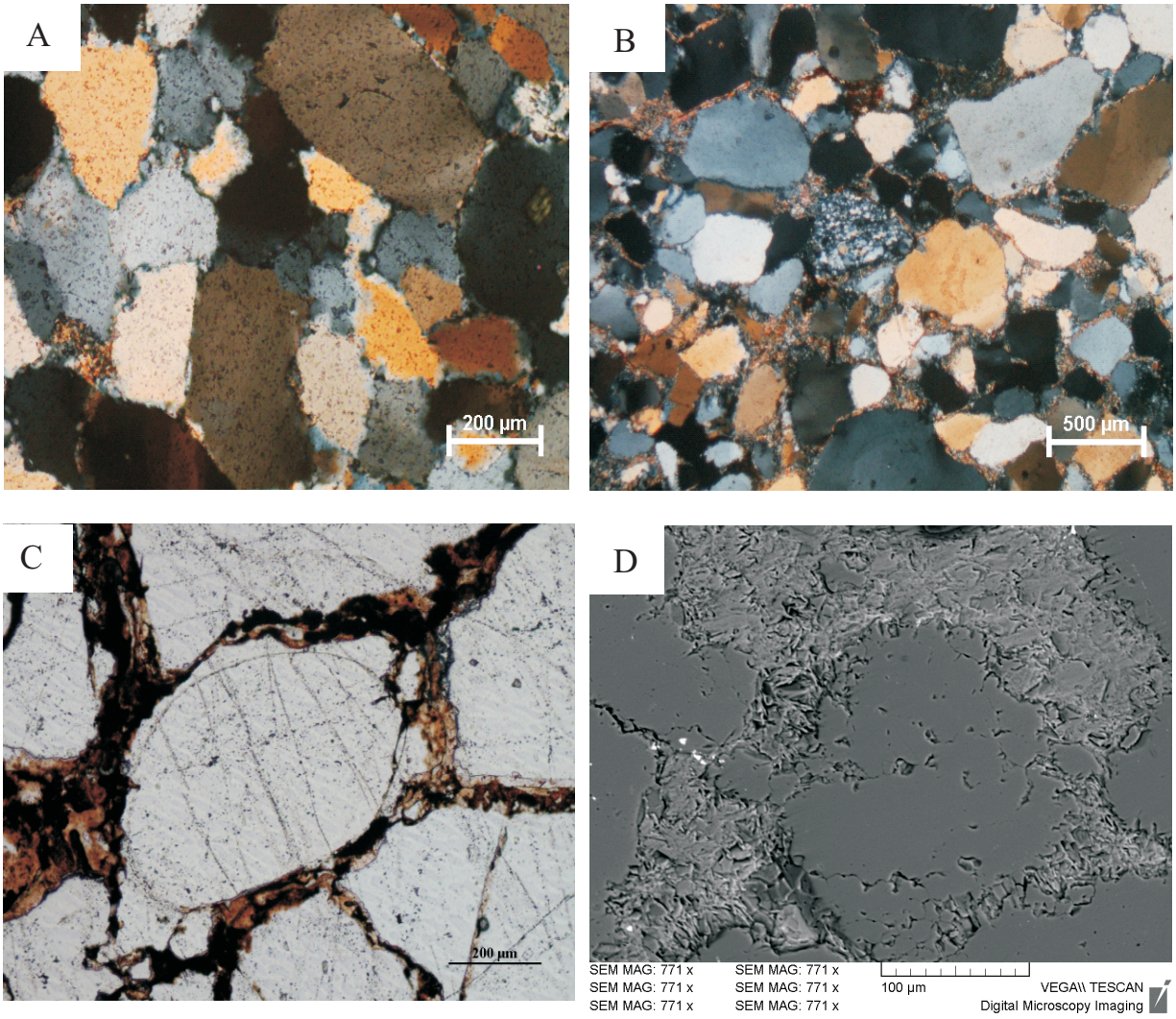

Figure.12.Optical and Scanning Electron micrographs of sandstones from Keonjhar Quartzite: (A) quartzarenite with sutured grain boundary in quartz framework population. (B) Quauartzite fragment within pseudomatrix. (C) Recycled well rounded quartz grain with syntaxial broken overgrowth. (D) Secondary matrix distribution around quartz grain.

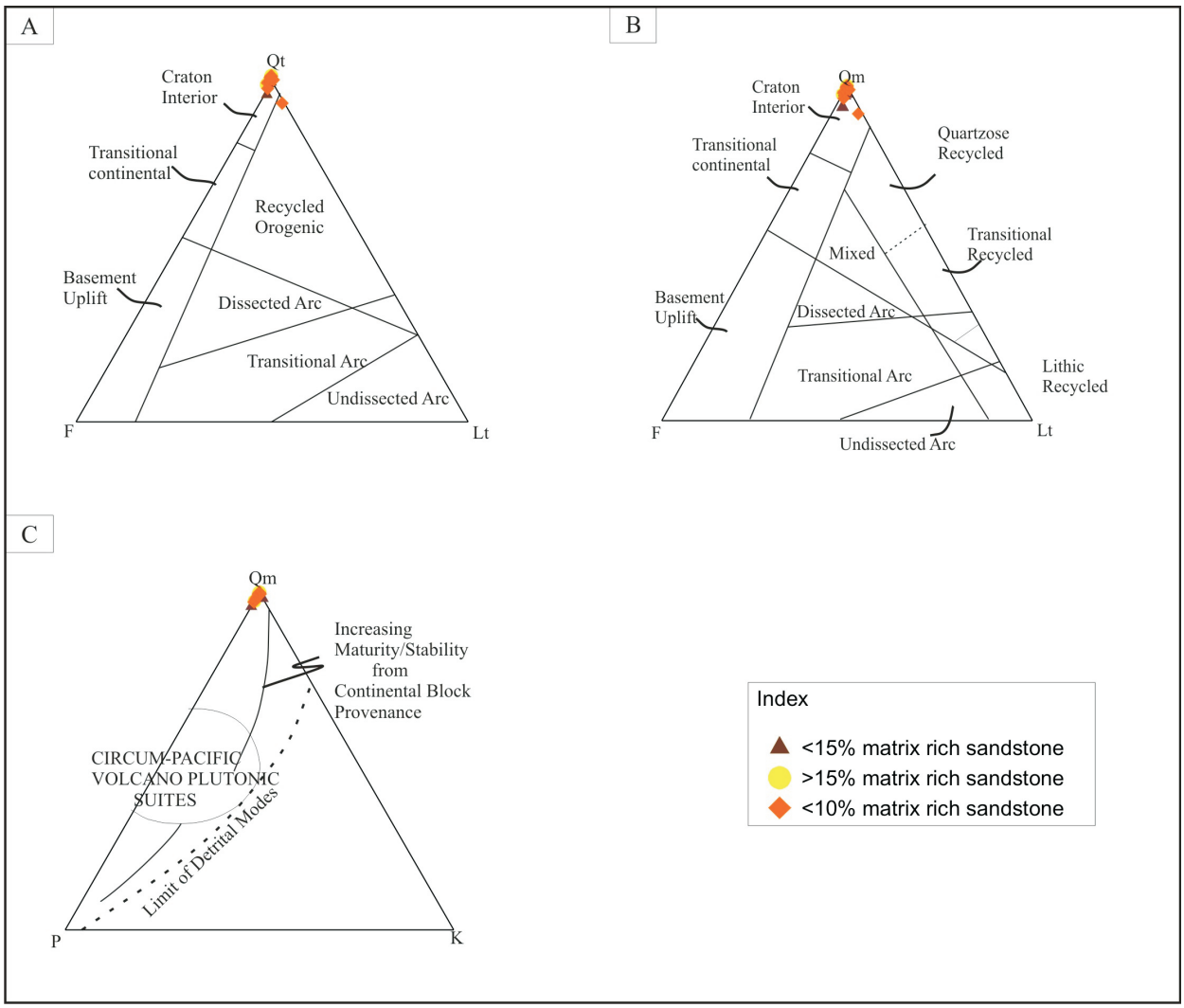

Figure. 13. (A) Qt-F-L compositional plots (after Dickinson and Suczek, 1979) of arenites. Note samples cluster in cratonic interior to recycled orogen fields. (B) Qm-F-Lt compositional plots (after Dickinson et al., 1983; Dickinson, 1985) of arenites. Note all the samples cluster in the quartzose recycled to cratonic interior origin. (C) Qm-P-K compositional plots (after Dickinson and Suczek, 1979) of arenites. Note all the samples cluster in the stable continental block provenance.

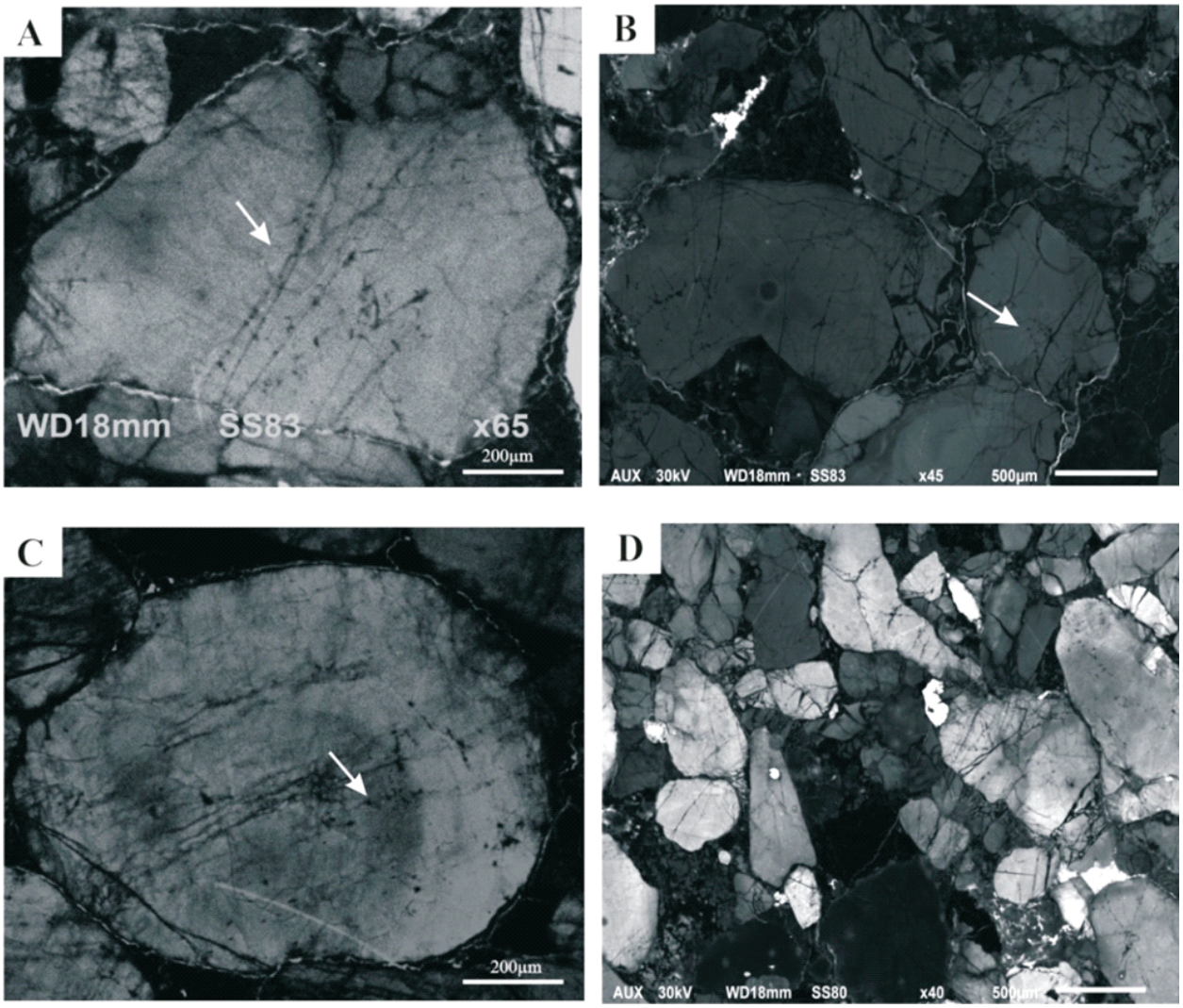

Figure. 14. SEM CL images of images of plutonic quartz from the Keonjhar Quartzite. (A) plutonic quartz with low luminescent and thin hairline healed fracture. (Note Healed fracture); (B) plutonic quartz where healed fracture filled by secondary fluid inclusion (foreign material or trace element like Li, Al, Ti) that produce dark streak and patches. (Note Healed fractures are filled by foreign material and produce dark patches);(C) Dark streak and patches in plutonic quartz grain; (D) Fractures are sparsely distributed and widely spaced as more than one set of lines. Note the fractures intersect at constant angles.

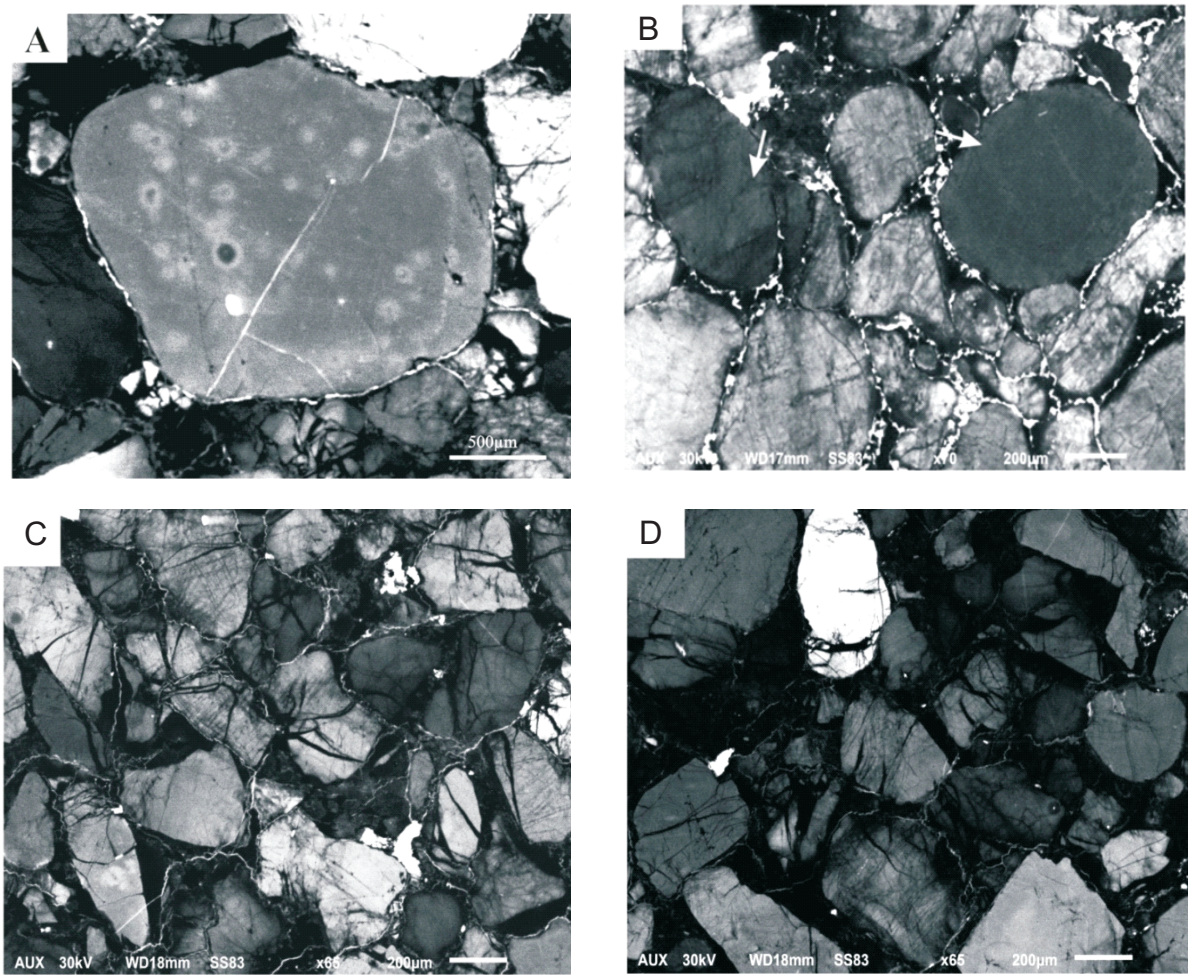

Figure.15. SEM CL images of low to medium grade metamorphic quartz from the Keonjhar Quartzite. (A) Inhomogeneous and patchy mottled luminosity in medium grade metamorphic quartz grain. (B) CL patterns of image of low grade metamorphic dominated detrital quartz population.(C) Medium-to-high grade deformed quartz grain produce brittle fracture. (D)Cathodoluminescence (CL) image of high-grade (bright luminosity) deformed quartz grain.

Roser and Korsch 1986; Fig. 16) indicate that the Keonjhar Quartzite was deposited in a passive margin tectonic setting.

Weathering and source area: CIA-PIA-ACNK-CIW (Fig: 17) moderate to very high values reflect the presence of both relatively unweathered and deeply weathered source rocks. Such a variation is likely to reflect the source rock components from multiple provenances.

Weathering Index	***Proposed by***	***Formula***	***Keonjhar sandstones (n =34)***	***Keonjhar QPC (n =13)***	***Keonjhar shales (n=3)***
CIA	(Nesbitt and Young, 1989)	Al_2O_3 x 100 /(Al_2O_3+CaO*+Na_2O+K_2O)	75-98 (Av. 82.80)	77-96 (Av. 87.47)	96-98 (Av.97.41)
CIW	(Harnois, 1988)	Al_2O_3 x 100 /(Al_2O_3+CaO*+Na_2O)	95 – 99 (Av.98.43)	98 – 99 (Av.98.91)	98.36-98.54 (Av.98.8)
PIA	(Fedo et al., 1995)	(Al_2O_3-K_2O) x 100 /(Al_2O_3+CaO*+Na_2O-K_2O)	95-99 (Av.98.79)	98.31-99.16 (Av.98.70)	98.46-99.35 (Av.98.78)

*La-Th-Sc and Th–Sc–Zr/10 (*after Bhatia andCrook 1986; Fig. 18): La-Th joins due to high concentration of La and Th. From this diagram it is implied that the sandstones here have typically granitic gneissic source. In Th-Sc-Zr/10 enrichment of Th in QPC samples denotes components from source close to the active continental margin.

Trace and REE compositions from the sandstones points towards a mixed source of felsic as well as mafic terrane (Fig. 19 and Fig. 20). This mixed source origin reveals the presence of both cratonic and recycled orogen provenance types. The presence of negative Eu-anomalies observed in most Keonjhar samples suggests major component of the provenance possibly was derived by intracrustal differentiation processes.

8. DETRITAL ZIRCON U-Pb-LU-Hf COMPOSITION OF KEONJHAR QUARTZITE

U-Pb and Lu-Hf compositions from detrital zircon in Meso-Neoarchean siliciclastic successions provide a robust database for distinguishing the relative proportion of juvenile and recycled plutons in the upper crust that constitute the provenance for such sediments. Lu-Hf composition from recently, dated 3.0 Ga Keonjhar Quartzite record detrital zircons from upper

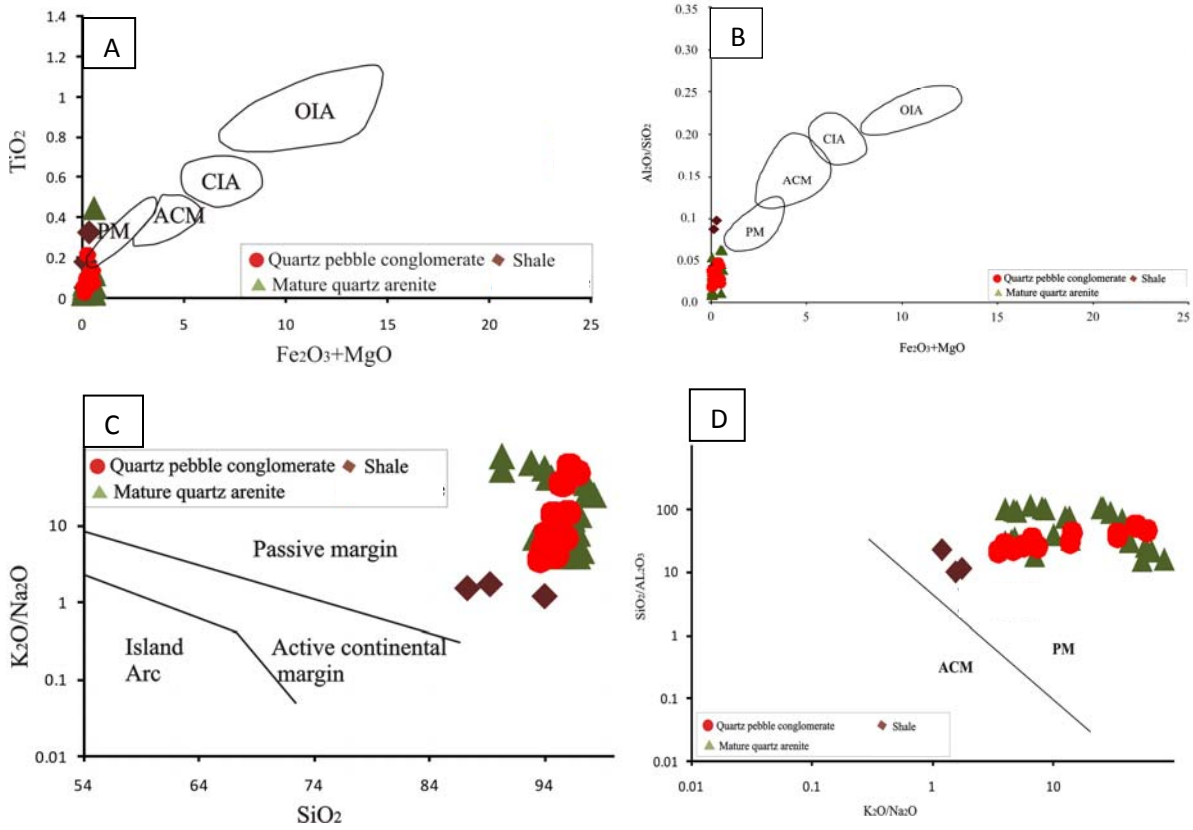

Figure. 16. Plots of major oxide composition from the Keonjhar Quartzite in different tectonic setting discrimination diagrams (after Roser and Korsch, 1986). (A) Plot in diagram using (Fe_2O_3 + MgO) versus (Al_2O_3/SiO_2). Note that the all samples plot very close to the fields of passive continental margins. (B) Plot in diagram using (Fe_2O_3 + MgO) versus TiO_2 content. Note that majority of the samples plot within and very close to the passive margin field. (C) Plot in SiO_2 versus K_2O/Na_2O Note that all of the samples Keonjhar Quartzite plot in the passive margin field. (D) Plot in SiO_2/Al_2O_3 versus K_2O/Na_2O diagram from major oxide data from the Mesoarchean sandstone in different tectonic setting discrimination diagrams (after Roser and Korsch, 1986). Note that all of the samples Keonjhar Quartzite plot in the passive margin field.

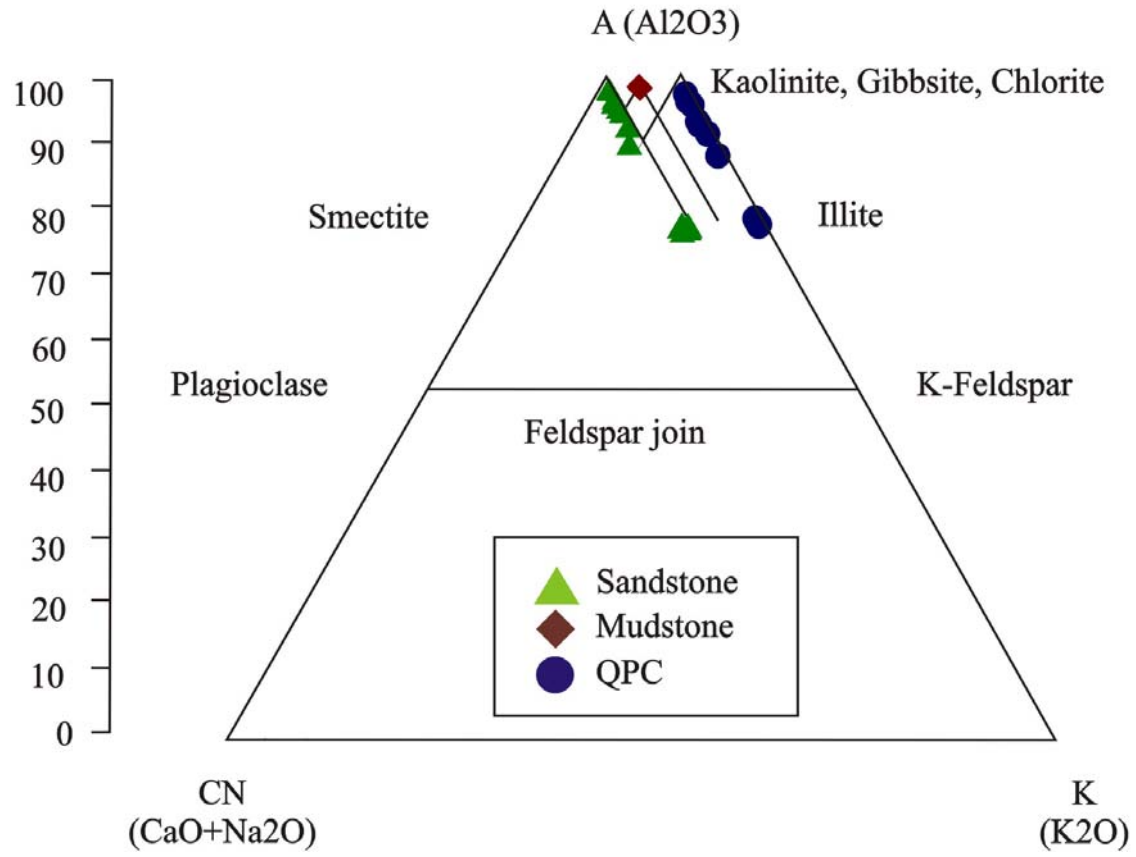

Figure. 17. Plots of major oxide composition in A-CN-K diagram (after Nesbitt and Young 1984). Note that the plots for the QPC, sandstone and mudstone samples show a distinct linear weathering trend parallel to the A-K side of the diagram.

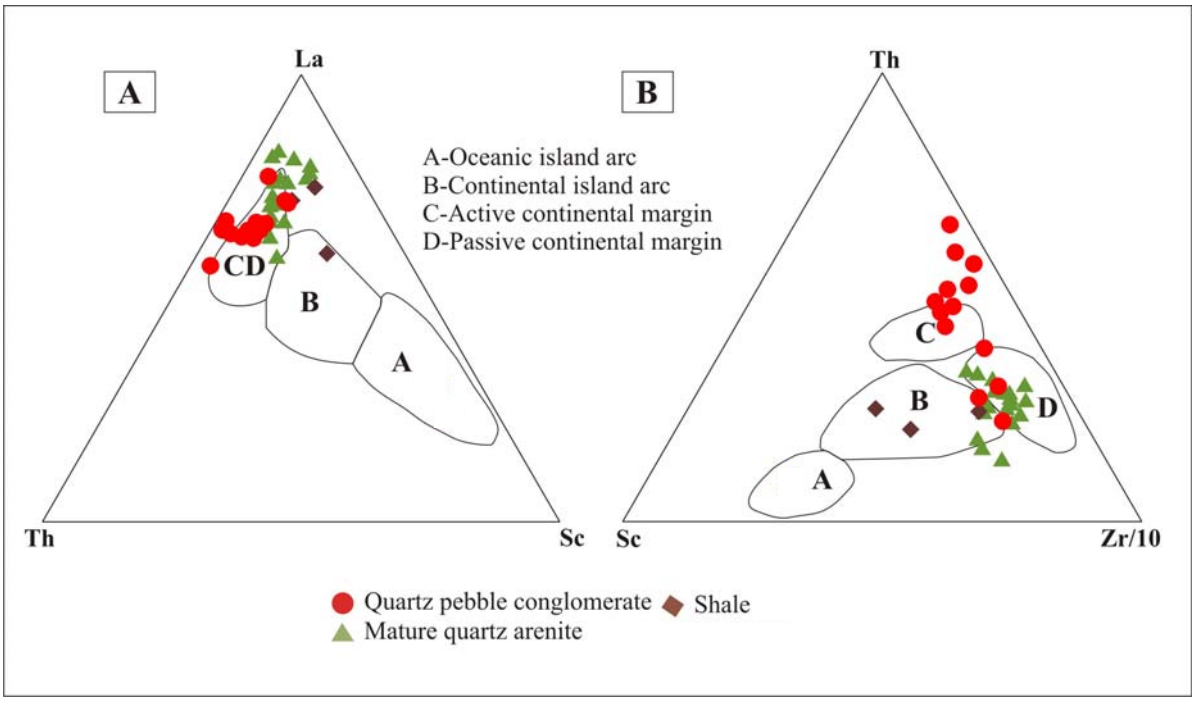

Figure. 18. (A) La–Th–Sc discriminatory plot (after Bhatia and Crook, 1986) for Mesoarchean Keonjhar Quartzite. Note that most of the samples plot within and close to the boundary of the fields of passive and active continental margin settings and three samples each from this formation plot in the field of oceanic island arc. (B) Th–Sc–Zr/10 discriminatory plot (after Bhatia and Crook, 1986) of Mesoarchean siliciclastics samples from the Keonjhar basin. Note that most of the siliciclastic samples plot within and close to the fields of both active and passive continental margins and three samples of this formation plot in the field of oceanic island arc.

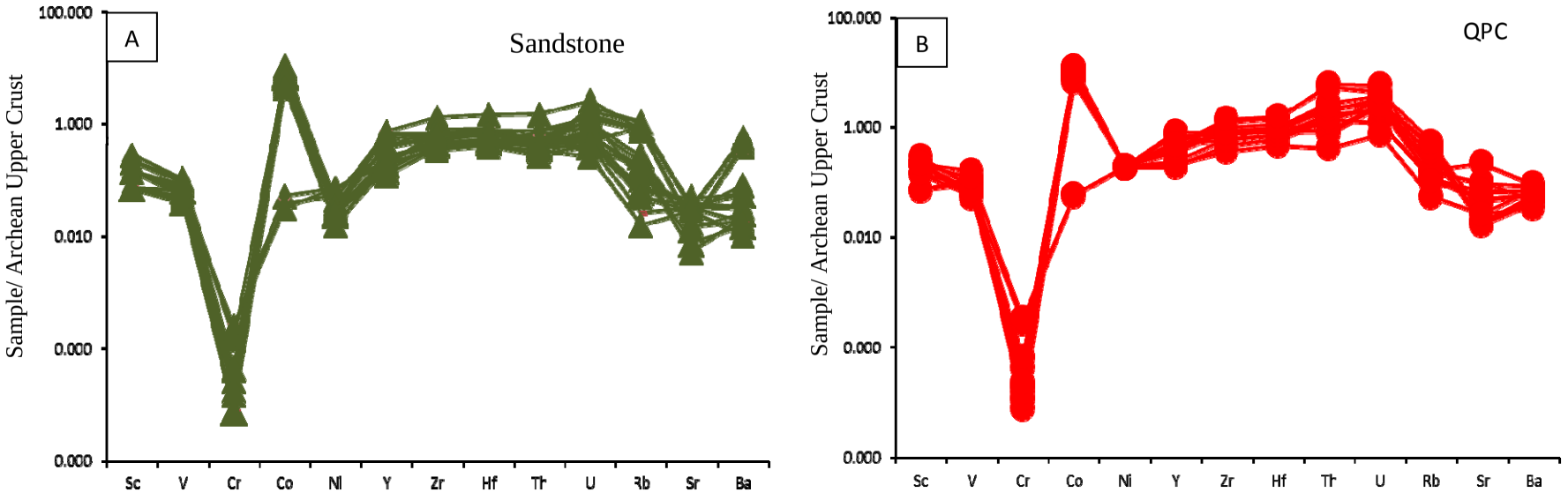

Figure. 19. Spider plots of trace element composition normalized with Archean upper crust (AUC) from the Mesoarchean Keonjhar Quartzite. (A)Trace elements normalized with Archean upper crust (AUC) with respect to sandstone. (B) Trace elements normalized with Archean upper crust (AUC) with respect to QPC.

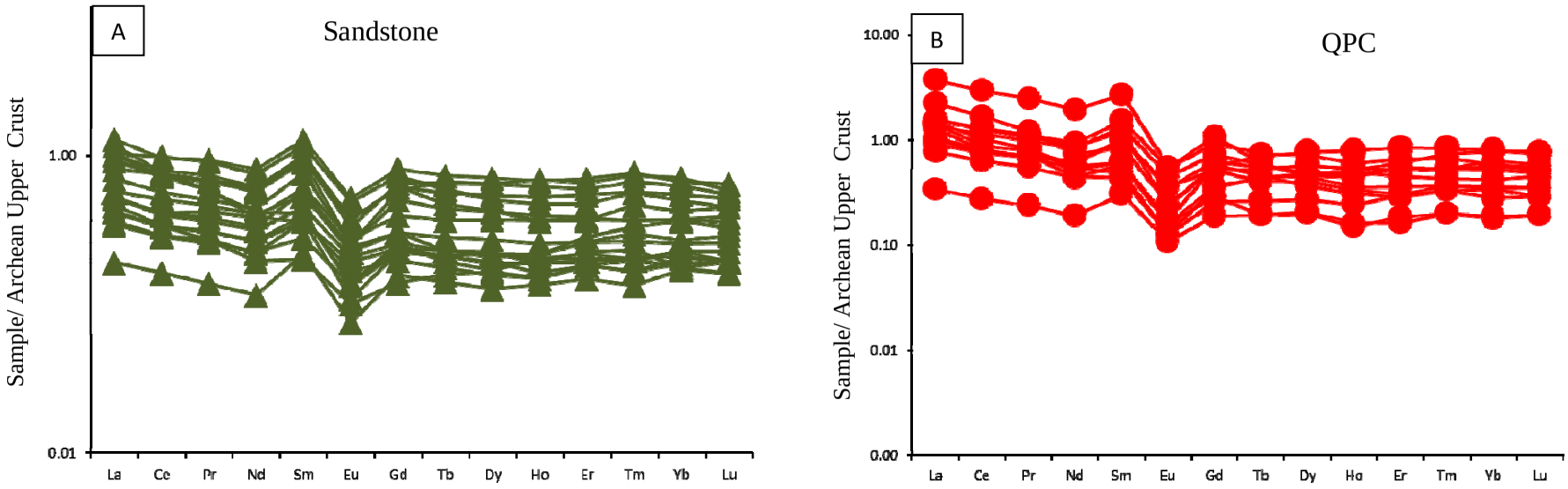

Figure. 20. Plots of Rare earth element (REE) composition normalized with Archean upper crust (AUC) from the Keonjhar Quartzite: (A) REE Compositions of sandstones. (B) REE compositions from QPCs (Quartz Pebble Conglomerate) within Keonjhar Quartzite.

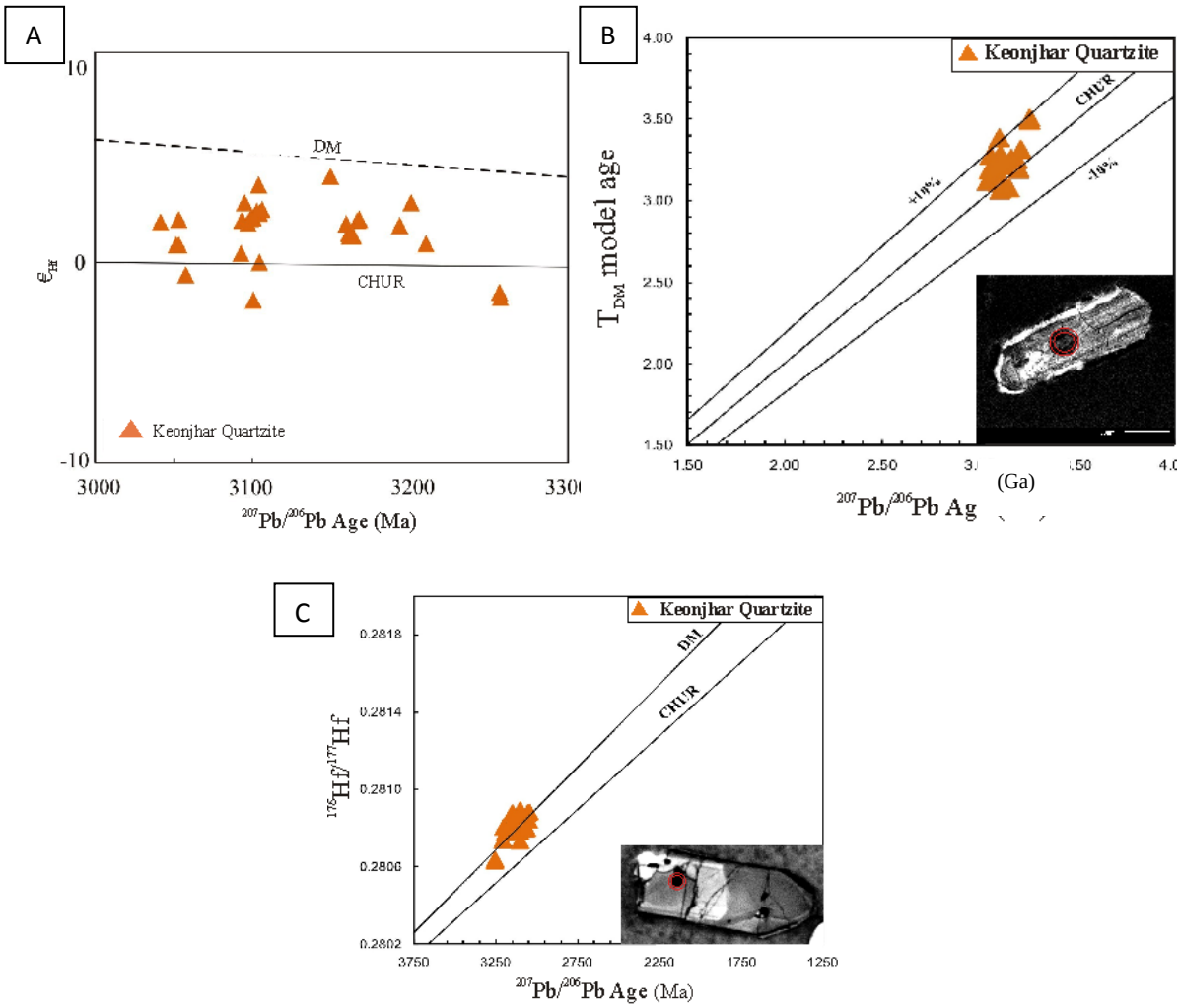

Figure. 21. (A) €$^{Hf(t)}$ versus $^{207}Pb/^{206}Pb$ Age(Ma) diagram showing results for detrital zircon from the Mesoarchean Keonjhar Quartzite (<3 Ga depositional age). (B) Detrital zircon T_{DM} model age vs $^{207}Pb/^{206}Pb$ Age (Ma) diagram. Note the Hf model age is much older than the crystallization age. (C) Detrital zircon $^{176}Hf/^{177}Hf$ versus $^{207}Pb/^{206}Pb$ Age (Ma) diagram showing that 'Juvenile continental crust' was dominant component in the granitoids at source of the sediments.

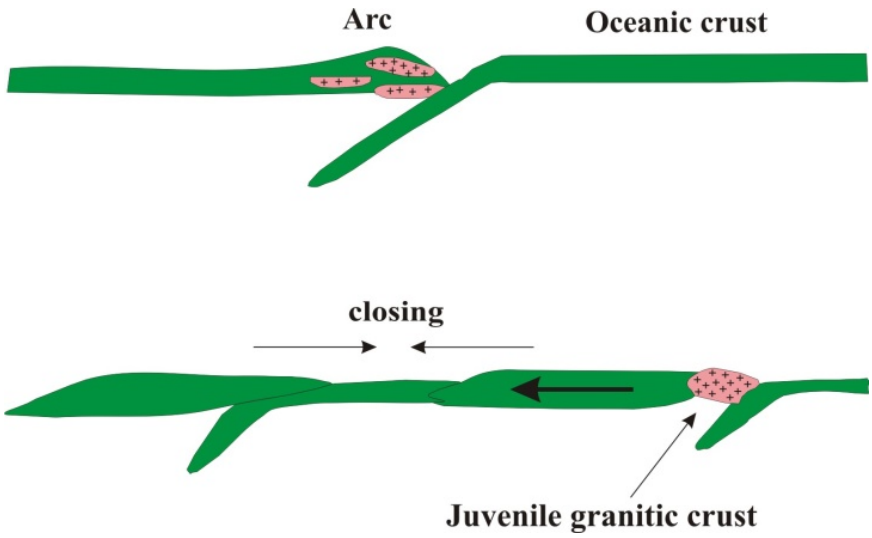

Figure. 22. Schematic diagram of accretionary orogen juvenile crust emplacement.

continental crust older than 3.0 Ga and reveals the proportion of juvenile/recycled crust in the Paleo-Mesoarchean Singhbhum Craton and explore the implications for early Archean geodynamics (Mukhopadhyay et al. 2014; Patchett et al. 1981).

The detrital zircon LA-ICPMS U-Pb-Lu-Hf compositions from the Keonjhar Quartzite was determined from sandstone samples in order to understand the source of early continental crust and its bearing on the geodynamics of Mesoarchean continental growth. ϵ_{Hf} isotopic compositions vary between -1.8 to +4.45 (2-sigma error). The zircons yield a predominantly superchondritic ϵ_{Hf} (+0.5 to +4.5), $^{176}Hf/^{177}Hf$=0.2808 and $^{176}Lu/^{177}Hf$=0.001 ratio. $\epsilon^{Hf(t)}$versus stratigraphic age plots reveals that the detrital zircons from Keonjhar Quartzite fall within the range of Depleted Mantle (DM) source (Fig. 21A ; Griffin et al. 2002). T_{DM} model age against stratigraphic ages suggest that T_{DM} model age of Hf of the zircon source is much older than their stratigraphic age (Fig. 21B). The superchondritic Hf isotopic compositions expressed as ϵ_{Hf} values, and $^{176}Hf/^{177}Hf$ against their stratigraphic ages suggest depleted mantle source and juvenile crustal components and possible onset of plate tectonics (Patchett et al. 1981; Fig. 21C and Fig. 22).

9. URANIUM MINERALIZATION IN KEONJHAR QUARTZITE

The radioactive quartz pebble conglomerates (QPC) in the Keonjhar Quartzite occur in the basal part of the succession. Radioactivity is recorded in two pebbly conglomerates in the basal part of the Asurkhol Member (Fig. 3). Brannerite, leucoxene, coffinite and thorite have been identified under SEM-EDS analyses (Fig. 23). Brannerite and leucoxene are the most abundant U-bearing mineral phase identified from some QPC clay pseudomatrix.

A comparative account of chemical compositions of the QPCs, sandstone (quartzite) in order to explore possible geochemical signals that might exist due to preferential concentration of radioactive minerals in the QPCs (Fig. 23A, 23B and 23C). I have also compared the composition of QPCs with composition of Singhbhum Granite to assess the source to sink differentiation of element composition that could be of importance for tracing the radioactive mineral potential of the QPCs. For the purpose of comparison I have normalized QPC compositions with respect to average sandstone composition of the Keonjhar Quartzite reported in this study and average composition of Singhbhum Granite from published database (Ref Saha 1994 and Dey et al. 2017).

Keonjhar Sandstone normalised diagram

Plot reveals that:

Major oxide:

1. Enrichment in Fe, Na, Ti and Mn and depletion in Mg, K in QPCs with respect to sandstones,
2. Little changes and closely constant proportion in Si, Al, Ca, and P in QPCs with respect to sandstones ,
3. Strong and irregular variation in Fe and K in QPC with respect to sandstone (Fig. 24A).

Trace element:

1. Enrichment in Cr, Ni, Th, U, Sr and Pb in QPCs with respect to the sandstone,
2. Depletion in Co, Rb, Cs and Ba in QPC samples with respect to the sandstone,
3. Comparable proportion in Cu, Zn, Ga, Y, Zr, Nb and Hf with respect to the sandstone (Fig. 24B).

Rare Earth Element:

1. enrichment in LREE in QPC samples with respect to the sandstone
2. Elevated Eu content with respect to sandstone and retention of negative Eu anomaly in QPC samples with respect to rest of the REE even after normalization wrt sandstone.
3. Comparable HREE proportion with respect to sandstone (Fig. 24C).

QPC composition normalised to Singhbhum Granite

When normalized with respect to Singhbhum Granite (composition after Saha 1994; Dey et al. 2017) the QPC reveals enrichment in Si, Al, Mn, K, Cu, Ga, Ni, Rb, V, Ta and LREE and depletion in Ca, Na, Cr, Pb, Sr, Y, with respect to the basement granitoids and little changes in Yb, Tb, Sm, Ce, Eu and Nd. Enrichment in Si, K, Rb and LREE are common changes from granitic basement to shelf sandstones of all ages as ascribed commonly due to the effect of weathering (Fig. 25, 26 and 27).

Implications for QPC-hosted Uranium mineralization

The geochemical and petrographic (including SEM) studies reveal that the radioactive mineralization of Mesoarchean Keonjhar QPC is composed of rutile/ uraniferous leucoxene aggregate associated with coffinite, thorite, uranothorite, zircon, pyrite and monazite. Detail study of the Mesoarchean Keonjhar QPC further reveals that rutile/leucoxene and uranium enriched brannerites are predominant mineral over all other uraniferous phase. U-Ti phases are restricted within QPC just above the unconformity. From external morphology, geochemical composition and core-rim structure, brannerite and all U-Ti phases speak in favour of

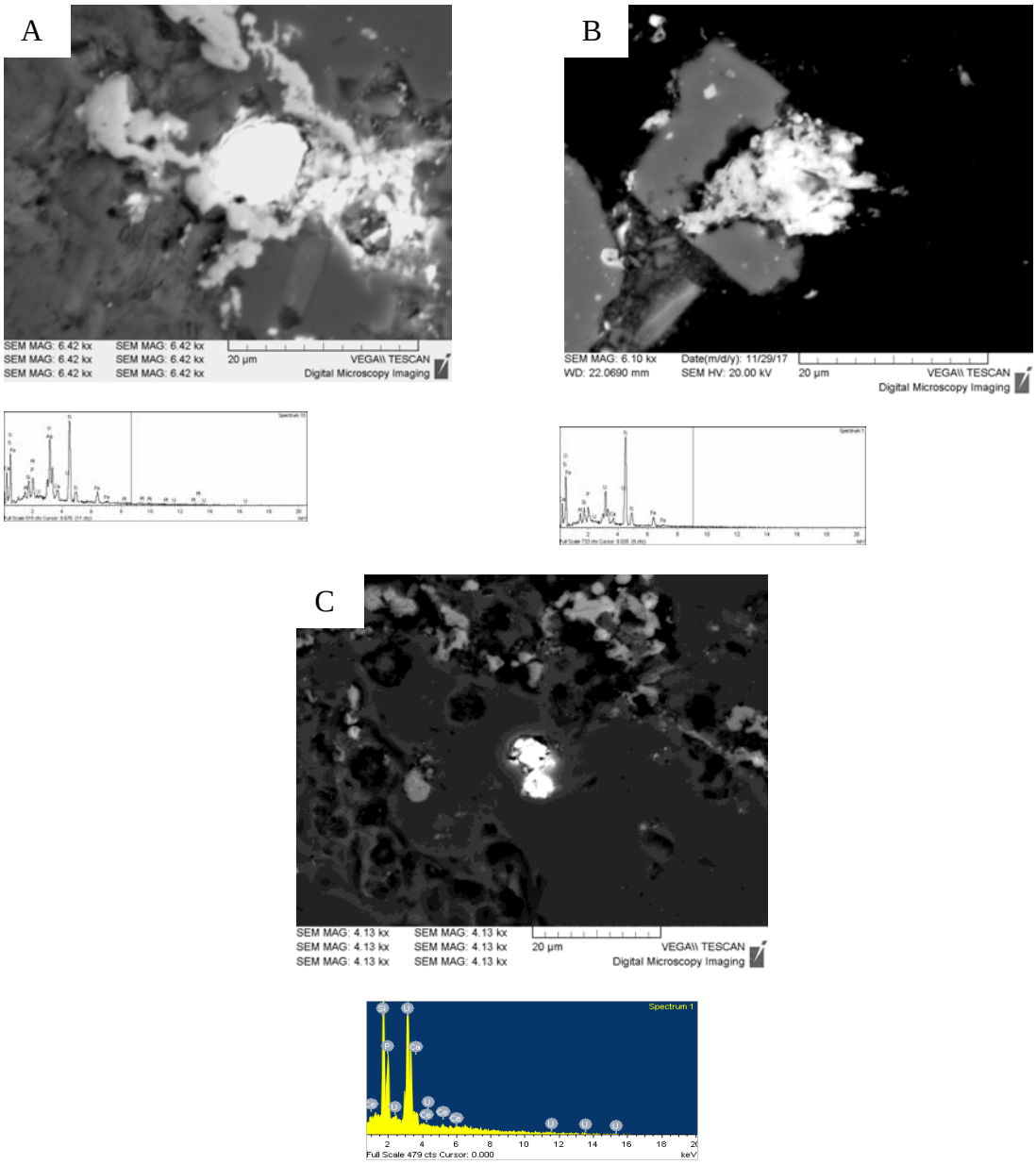

Figure. 23. (A)SEM- images of Brannerite grain from QPC samples of Keonjhar Quartzite. (B) SEM- EDS analysis of uraniferous leucoxene grain from QPC samples of Keonjhar Quartzite. (C) SEM- EDS analysis of Uraniferous leucoxene grain from QPC samples of Keonjhar Quartzite.

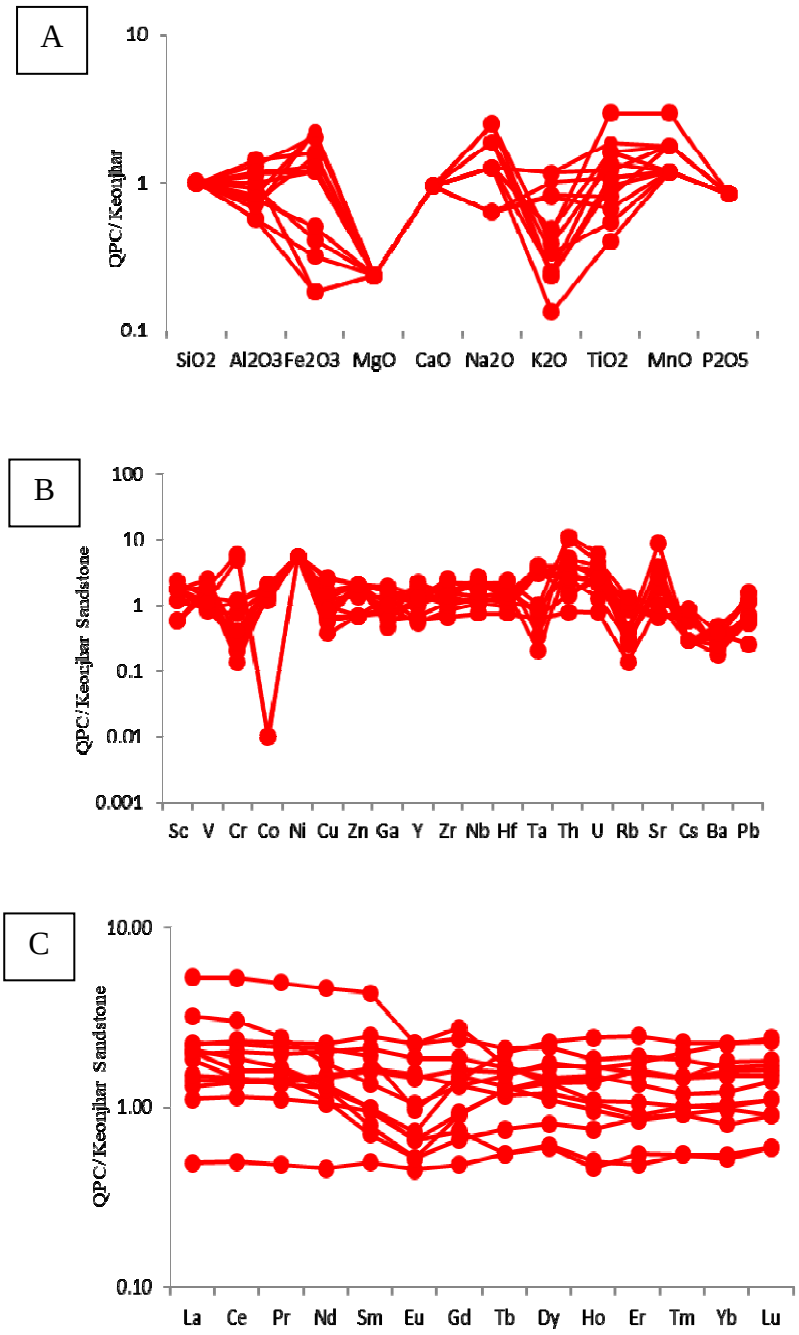

Figure. 24. Keonjhar QPC plots plot normalised with respect to sandstones (A) Major oxide variations Note: variable enrichment in Fe_2O_3, Na_2O, TiO_2 and MnO and depletion in MgO, K_2O and P_2O_5. (B) Trace element spider plot Note Enrichment in Cr, Ni, Th, U, Sr and Pb in QPC and depletion in Co, Rb, Cs and Ba. (C) REE Plots. Note enrichment in LREE in QPC and retention of negative Eu-anomaly.

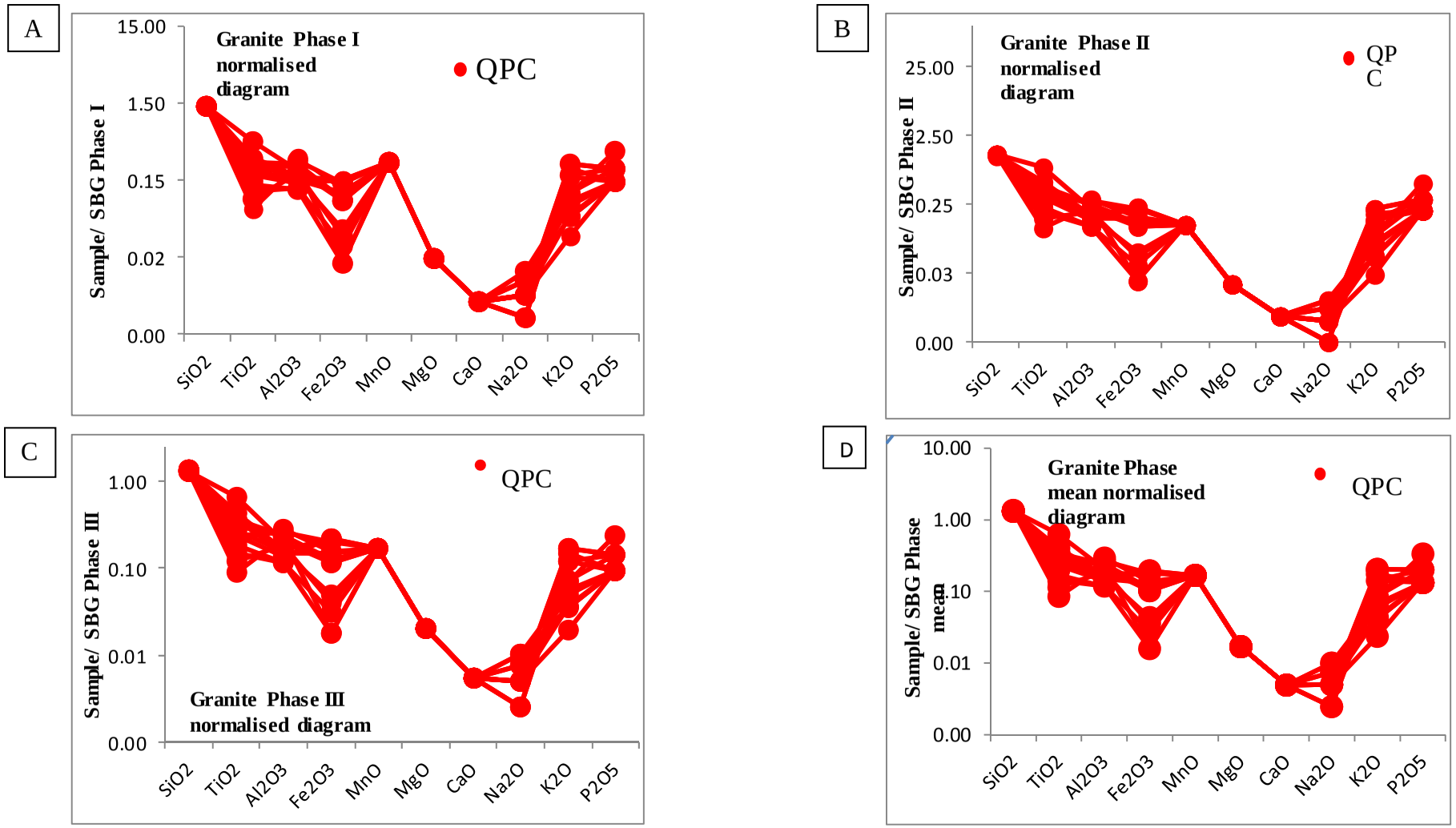

Figure. 25. Plots of QPC major oxide data from the Keonjhar Quartzite (A) Major oxide normalized diagram with Singhbhum Granite phase I. (B) Major oxide normalized diagram with Singhbhum Granite phase II. (C)Major oxide normalized diagram with Singhbhum Granite phase III. (D)Major oxide normalized diagram with Singhbhum Granite (mean of all phases).

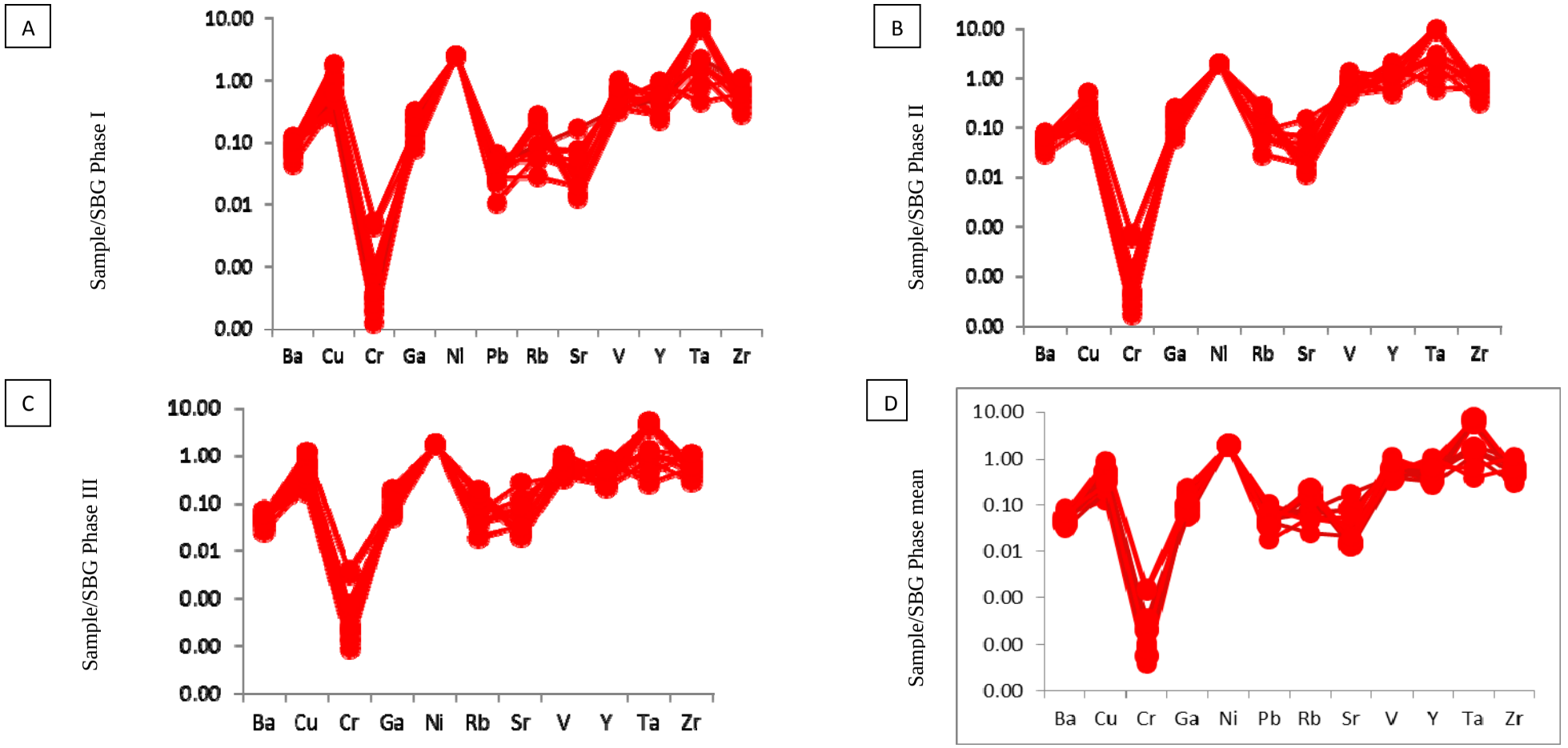

Figure. 26. Plots of QPC trace elements data from the Keonjhar Quartzite. (A) Trace element data normalized diagram with Singhbhum Granite phase I. (B) Trace elements data normalized diagram with Singhbhum Granite phase II. (C) Trace elements data normalized diagram with Singhbhum Granite phase III. (D)Trace elements data normalized diagram with Singhbhum Granite phase mean (mean of all phases).

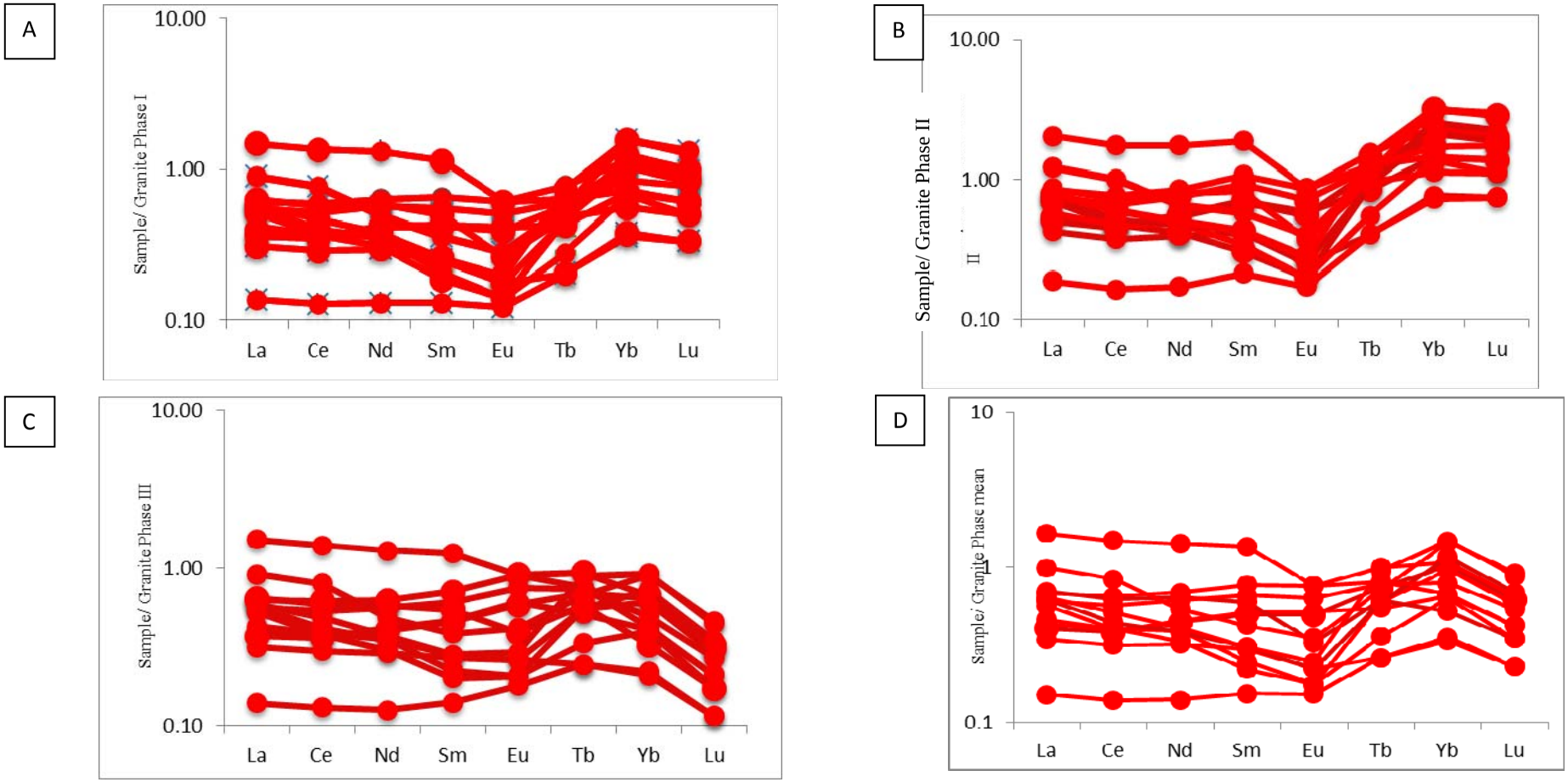

Figure. 27. Plots of REE from the Keonjhar Quartzite (A) Rare Earth elements data normalized diagram with Singhbhum Granite phase I. (B) Rare Earth elements data normalized diagram with Singhbhum Granite phase II. (C) Rare Earth elements data normalized diagram with Singhbhum Granite phase III. (D)Rare earth elements data normalized diagram with Singhbhum Granite (mean of all phases).

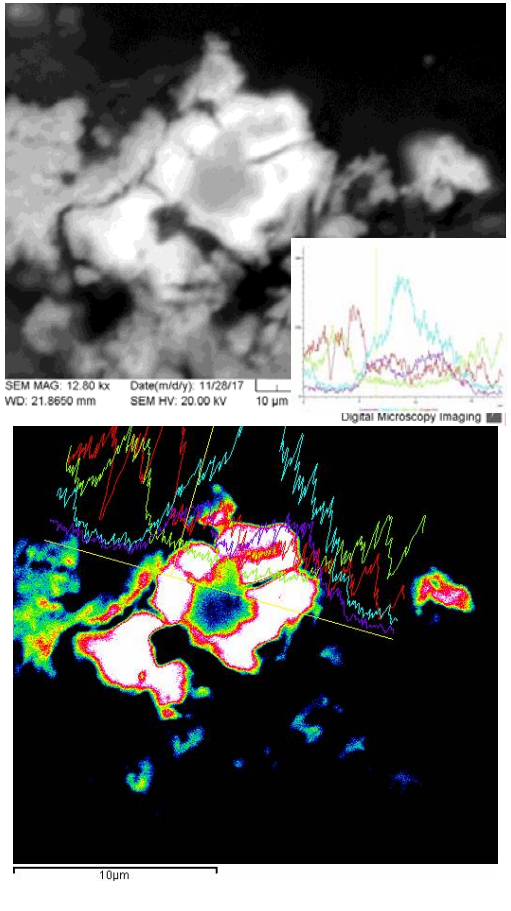

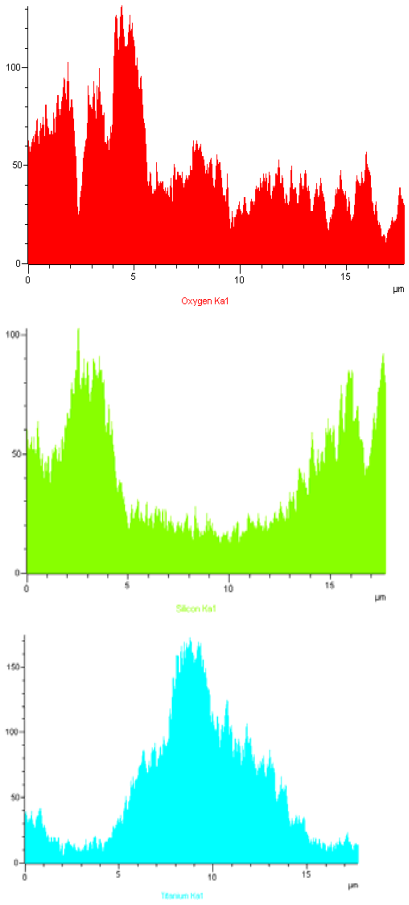

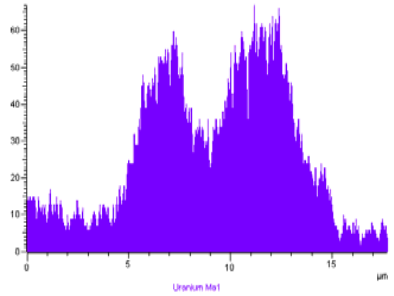

	Rutile	Leucoxene	Brannerite
Oxides	Compd%		
SiO_2	2.79	3.45	26.07
P_2O_5	1.86	3.87	4.5
CaO	0.89	1.2	1.79
TiO_2	82.33	69.05	31.05
FeO	3.9	5.01	5.98
UO_3	8.23	17.42	30.62

Figure. 28. SEM- EDS images and analyses of corona texture (rutile in the core of texture and brannerite in the rim) from Pronto Reaction.

	U	Th	SiO_2	Al_2O_3	Fe_2O_3	Na_2O	K_2O	MnO	TiO_2
U	1								
Th	0.883	1							
SiO_2	-0.173	0.129	1						
Al_2O_3	-0.016	-0.281	-0.972	1					
Fe_2O_3	0.484	0.355	-0.401	0.274	1				
Na_2O	-0.042	-0.286	-0.789	0.808	0.2	1			
K_2O	0.239	0.44	0.638	-0.75	0.105	-0.571	1		
MNO	0.775	0.825	0.14	-0.242	-0.003	-0.245	0.26	1	
TiO_2	0.982	0.873	-0.236	0.058	0.437	-0.011	0.13	0.8	1

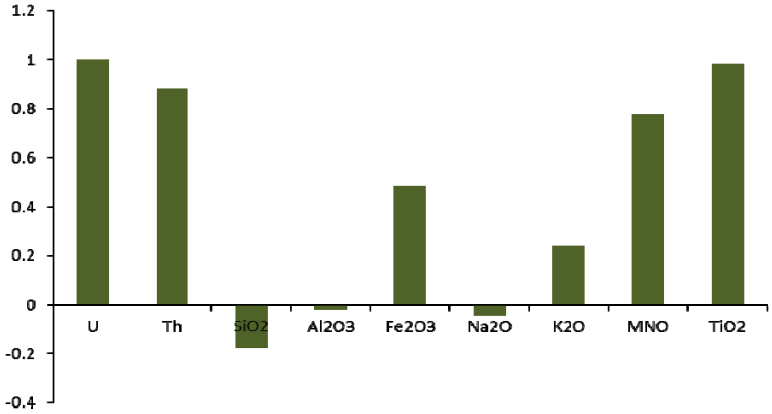

Figure. 29. Matrix correlation diagram of U-Th composition and major oxides.

	U	Sc	V	Cr	Co	Cu	Ga	Y	Zr	Ti	Nb	Hf	Ta	Th	Rb	Sr	Ba	Pb
U	1																	
Sc	0.162	1																
V	-0.16	-0.168	1															
Cr	0.226	0.37	0.029	1														
Co	-0.235	-0.053	-0.046	-0.848	1													
Cu	0.229	0.519	-0.136	0.916	-0.643	1												
Ga	0.139	-0.022	0.391	-0.334	0.101	-0.507	1											
Y	0.255	0.436	-0.255	0.465	-0.468	0.527	0.039	1										
Zr	0.886	0.292	-0.079	0.473	-0.511	0.391	0.236	0.319	1									
Ti	0.982	0.062	-0.121	0.149	-0.211	0.123	0.199	0.229	0.831	1								
Nb	0.478	0.435	0.211	-0.248	0.301	-0.177	0.641	0.288	0.41	0.472	1							
Hf	0.875	0.259	-0.119	0.499	-0.549	0.389	0.221	0.33	0.991	0.829	0.342	1						
Ta	-0.151	0.195	0.214	-0.434	0.746	-0.264	0.14	-0.222	-0.331	-0.16	0.499	-0.386	1					
Th	0.883	0.057	-0.176	0.459	-0.45	0.388	-0.136	0.109	0.829	0.873	0.089	0.848	-0.359	1				
Rb	0.21	0.622	-0.281	0.773	-0.465	0.903	-0.638	0.33	0.352	0.095	-0.185	0.338	-0.198	0.41	1			
Sr	0.694	-0.405	-0.165	-0.363	0.126	-0.426	0.309	-0.052	0.425	0.776	0.359	0.432	-0.021	0.552	-0.426	1		
Ba	0.689	-0.007	-0.029	-0.002	-0.005	-0.043	0.347	0.182	0.588	0.715	0.599	0.568	0.268	0.567	-0.06	0.706	1	
Pb	0.265	0.244	0.173	-0.339	0.18	-0.354	0.843	0.331	0.279	0.277	0.824	0.236	0.188	-0.152	-0.466	0.309	0.318	1

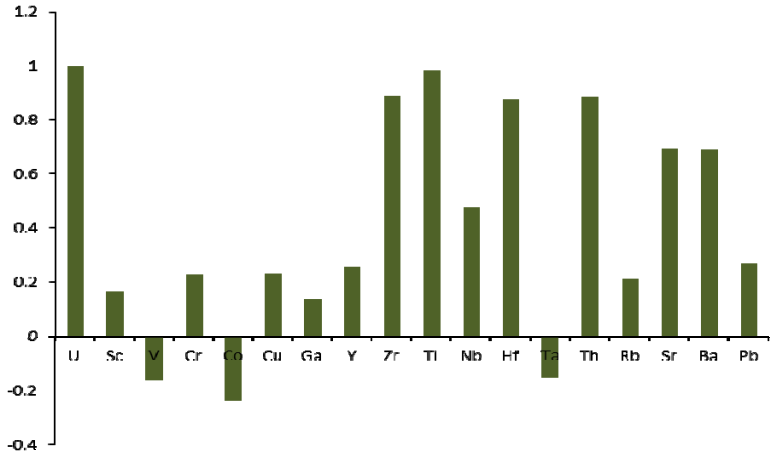

Figure. 30. Matrix correlation diagram U-Th correlation with trace elements.

	U	Th	La	Ce	Pr	Nd	Sm	Eu
U	1							
Th	0.883	1						
La	0.944	0.924	1					
Ce	0.946	0.895	0.989	1				
Pr	0.934	0.846	0.978	0.993	1			
Nd	0.894	0.736	0.916	0.954	0.979	1		
Sm	0.824	0.599	0.815	0.877	0.915	0.971	1	
Eu	0.634	0.305	0.55	0.636	0.675	0.763	0.877	1

	U	Th	Gd	Tb	Dy	Ho	Er	Tm	Yb	Lu
U	1									
Th	0.883	1								
Gd	0.77	0.498	1							
Tb	0.594	0.37	0.805	1						
Dy	0.384	0.24	0.574	0.936	1					
Ho	0.29	0.175	0.447	0.882	0.976	1				
Er	0.248	0.199	0.341	0.814	0.949	0.974	1			
Tm	0.294	0.268	0.318	0.788	0.94	0.95	0.978	1		
Yb	0.305	0.31	0.23	0.703	0.87	0.902	0.948	0.974	1	
Lu	0.344	0.348	0.264	0.722	0.875	0.902	0.935	0.97	0.993	1

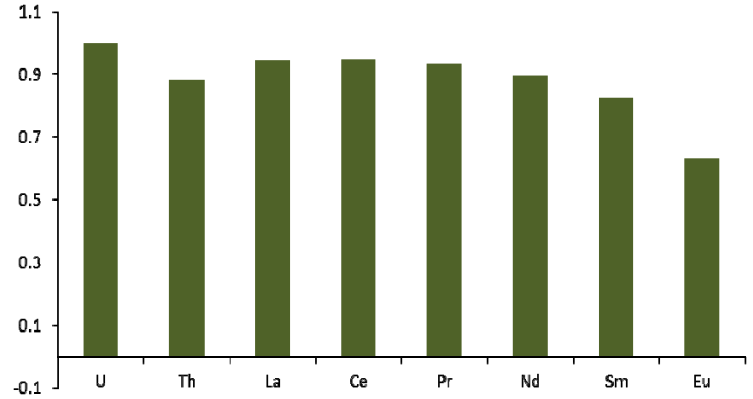

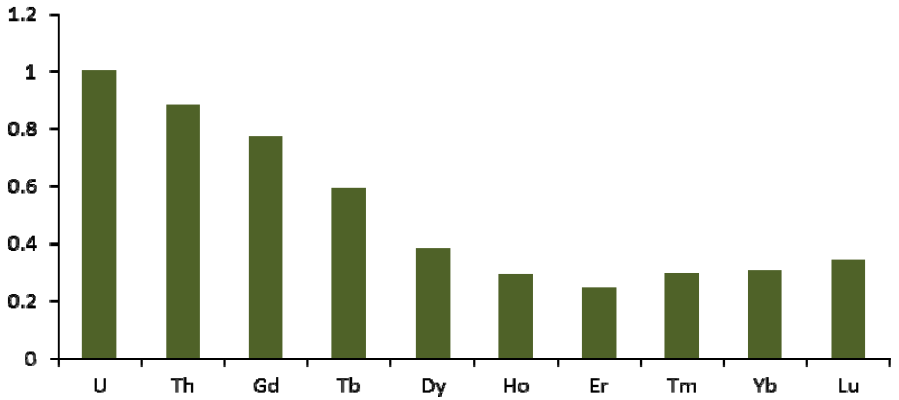

Figure. 31. Matrix correlation diagram U-Th correlation with rare Earth elements.

diagenetic alternations (Fig. 28). Correlations of concentration of U and Th wrt other elements (Fig. 29, 30 and 31) reveal positive correlation with TiO_2, Zr, and Hf. Correlations with Ti, Zr and Hf in turn suggest that uranium concentration is related to the concentration of detrital rutile and hence detrital zircon. A low positive or no correlation of U with redox sensitive elements (V, Cr, and Cu) may indicate that U- here is not associated with redox sulphides common to detrital uraninite redox placers. U also reveals positive correlation with LREEs indicating preferential U-concentration in supergene phosphate phases. The elemental correlations of U and other elements are likely to suggest U-mineralization took place in the supergene weathering profile through alteration of Ti-bearing phases (*Pronto Reaction*). Such signature may be important in understanding hidden redox U-paleoplacers below the supergene weathering profile.

10. **DETRITAL IRON ORE DEPOSITION KEONJHAR QUARTZITE**

The iron ore conglomerate body in the Keonjhar Quartzite occurs in the upper part of the succession. The iron ore conglomerate body occur in ~40 m thick incised valley fill deposit within shelf environment. The iron ore clasts are so predominant component in these conglomerates, that the conglomerates are mined as low-grade iron ores. The conglomerates are very unique in a sense that they are encased in a shelf sandstone host succession and the ore clasts are remarkably similar with the hard laminated or hard massive ores of the neighbouring BIF-hosted high-grade deposits of the Noamundi-Joda iron ore district (Fig. 32). The deposits have been described in Mukhopadhyay et al (2007) and based on stratigraphic consideration a Neoarchean to Paleoproterozoic age of the conglomerates was suggested by Mukhopadhyay et al. (2007). In the present work I have attempted to constrain the age of deposition from the conglomerates from detrital zircon U-Pb ages from the sandstone clasts in the conglomerates.

Mode of occurrence of the Iron Ore Conglomerates

The iron ore clast-bearing conglomerates occur as amalgamated lensoid mass-flow deposits incised within mature shallow shelf succession. The clast size varies among lenses and range from cobble/boulder size to pebble size. Clasts include hard hematitic iron ore, BIF and sandstones. The ore conglomerate bearing interval is about 40 m thick and 220 m along the strike.

Iron ore petrographic description

The lensoid iron conglomerate deposit is encountered at surface near Chamakpur region. This iron conglomerate is practically not affected by supergene alteration. The predominant ore

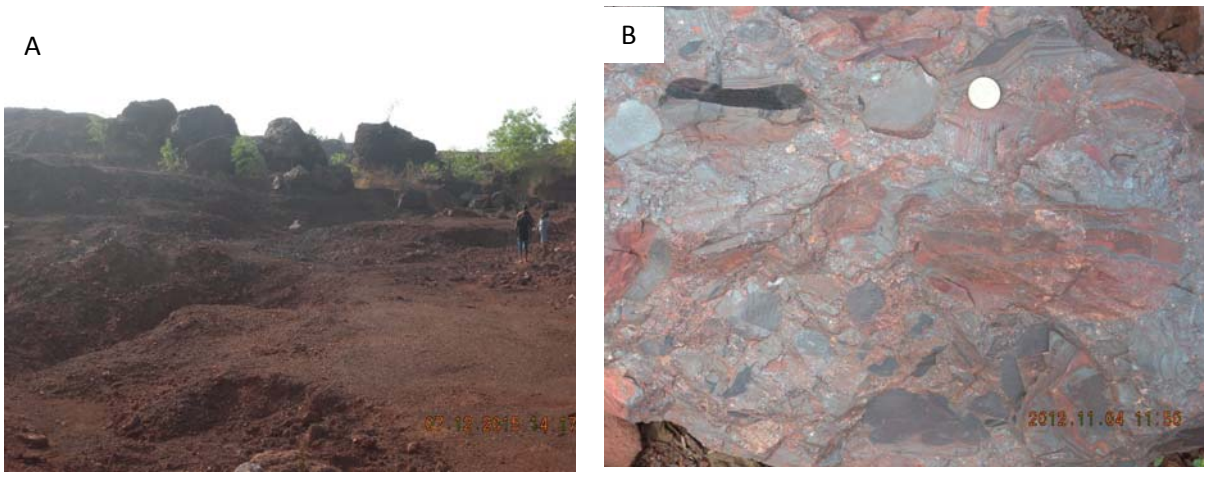

Figure. 32. (A) Field photograph of lensoid iron ore conglomerate bodies mined out from Chamakpur Member. (B) Field photograph of iron ore conglomerate with clasts of hard iron ore (dark steel gray) and BIF (reddish) in Chamakpur Member. Note well rounded hard iron ore clast (near the left upper corner coin scale).

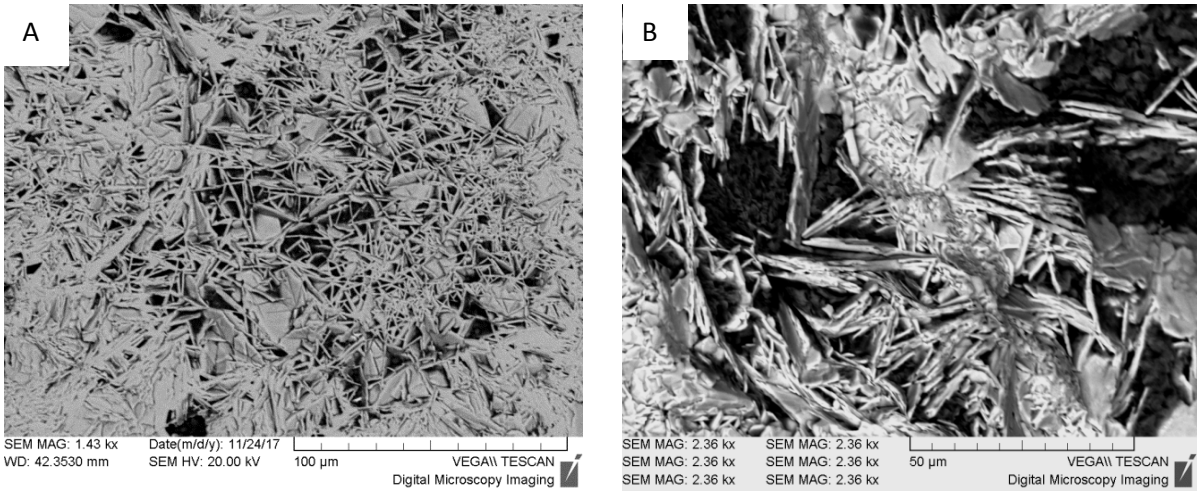

Figure. 33. BSE-SEM images of ore texture from clast of iron ore from iron ore bearing conglomerates (A) Anhedral and microplaty hematite. (B) Martite distribution surrounded by microplaty hematite.

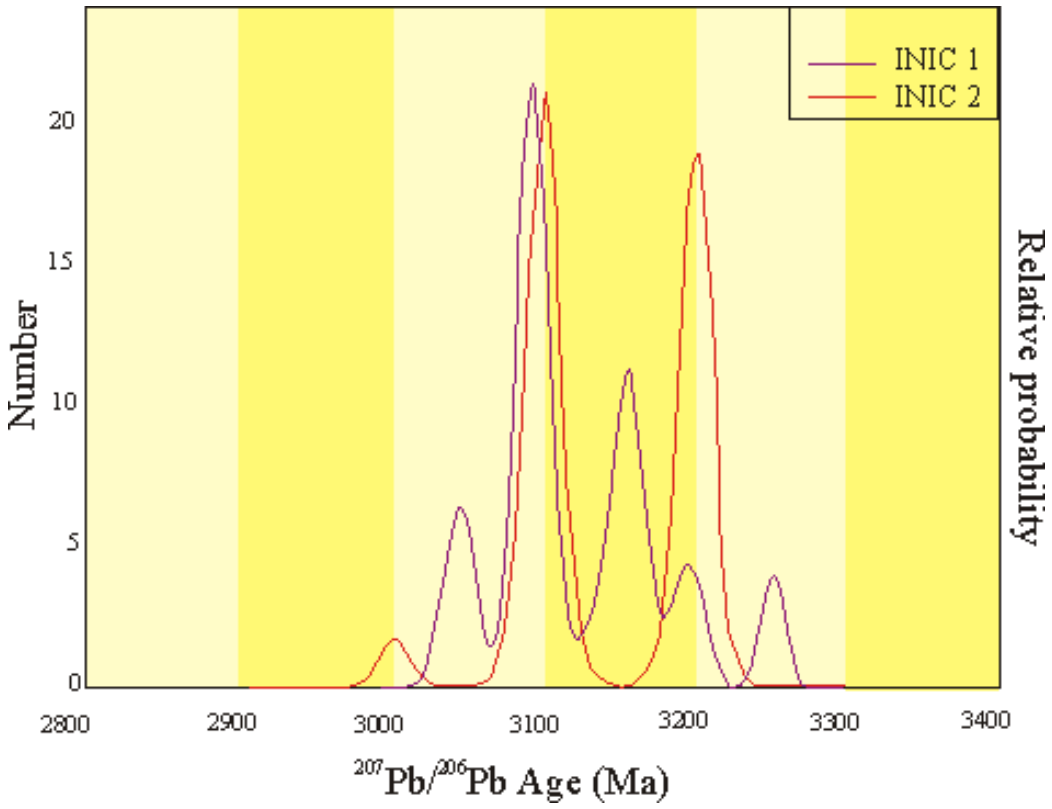

Figure. 34. Detrital zircons LA-ICPMS U-Pb age ranging from 3.0–3.3 Ga (considered those zircons with <5% discordance limit) from sandstone clasts in iron ore conglomerate and overlying sandstone beds of Keonjhar Quartzite.

minerals in iron oxides bands are anhedral, and microcrystalline hematite/ magnetite. The matrix of the iron conglomerate is mainly massive crypto- to microcrystalline hematite, partially oxidized magnetite and detrital quartz (Fig. 33).

Detrital Zircon U-Pb ages from sandstone clasts in the conglomerates

The U-Pb data detrital zircons are mainly magmatic nature with oscillatory zoning. The age population of these zircons is shown in a histogram (Fig. 32). The U-Pb age represents the $^{207}Pb/ ^{206}Pb$ maximum depositional age for zircons. The zircons from sandstone clasts of the iron ore conglomerate body shows maximum depositional age of 3.0 Ga (considered those zircons with <5% discordance limit, Fig. 34) and also suggests that the primary hard iron ore formation age at source deposits from where the clasts were derived is at least older than 3.0 Ga.

Controls on iron ore conglomerate deposition

The detrital zircon ages from the sandstone clast of the iron ore conglomerate suggest that iron ore mineralization in their source of these conglomerates predated the depositional age of the host Keonjhar Quartzite succession and fixes the lower limit of the ore formation at around 3 Ga. The deposition of the conglomerate within shelf sandstone is in fact difficult to explain. The conglomerate in shelf sandstone marks a major base level fall and fluvial incision on the wave-agitated shelf. The fluvial incision in shelf implies a condition of forced regression. Forced regression on the other hand is a result of combining effect of eustatic fall and tectonic uplift. In case of the Chamakpur iron ore conglomerates the base level fall in the upper part of the Keonjhar Quartzite succession may be due to such eustatic and tectonic factors.

11. **CONCLUSIONS**

The Keonjhar siliciclastics studied in the North of Keonjhar Town represents one of the best preserved examples of sedimentation during Mesoarchean time. The succession is dominated by mature quartz arenite *albiet* modified to quartzite with low greenschist grade metamorphism. Based on the mappability and distinct lithology the succession is classified here as a formal lithostratigraphic unit of the rank of formation and named as Keonjhar Quartzite. Two members have been proposed here within the Keonjhar Quartzite, namely, the Asurkhol Member that forms the lower conglomerate-pebbly sandstone-coarser sandstone dominated part of the succession and a *lentil* of iron ore clast-bearing conglomerate at the upper part of the succession, namely, Chamakpur Member. Based on lithology, grain size and

primary sedimentary structures nine sedimentary facies have been identified. Facies analysis reveals that the lower part of the succession is dominated by mass-flow deposits of conglomerates from proximal subaerial fan depositional association. The mass-flow conglomerate-dominated association grades upward to cross-stratified and wavy bedded mature arenite succession of shallow marine wave-agitated shelf depositional setting. Paleocurrent pattern is dominantly unimodal WSW-ly with locally preserved bipolar distribution. Internal organization of sandstone beds into sets and cosets of trough/planar cross-strata and wave-reworked upper bounding surfaces of the sandstone beds together with the paleocurrent pattern testify to tidal influence in the sand accumulation and dispersal. The facies sequence can be described in terms of a depositional sequence. The sequence initiating over unconformity on the Singhbhum Granite and IOG greenstones includes a lowermost LST with incised Valley Fills from FSST. This is followed by a TST and aggradational phase of TST-HST. Petrographic study reveals craton interior to recycled orogen sources and the geochemical proxies using major, trace-REE analyses suggest a passive margin setting with cratonic as well as active margin components in the provenance. The REE pattern with negative Eu-anomaly indicates the presence of differentiated upper crust during Mesoarchean in the Singhbhum craton. The superchondritic Hf isotopic compositions expressed as ϵ_{Hf} values against their stratigraphic ages from the detrital zircon LA-ICPMS U-Pb-Lu-Hf compositions suggest depleted mantle source and juvenile crustal components and possible onset of accretionary plate tectonics. The iron ore conglomerate in the upper part of the succession is interpreted as product of a forced regression in this profile. The hard ore clasts in the conglomerate suggest that the ore formation in the source terrane predated the deposition of the conglomerate and hence should be >3.0 Ga event. Uranium mineralization in the basal QPCs reveals U-concentration in the U-Ti oxides and U-Th-phsophates and indicates supergene mobilization of U in the shallower profiles.

REFERENCES

Acharyya, S. K., Gupta, A., and Orihashi, Y., 2010. Neoarchean–Paleoproterozoic stratigraphy of the Dhanjori basin, Singhbhum Craton, Eastern India: And recording of a few U–Pb zircon dates from its basal part. Journal of Asian Earth Sciences, 39, 527-536.

Beukes, N. J., Mukhopadhyay, J., and Gutzmer, J., 2008. Genesis of high-grade iron ores of the Archean Iron Ore Group around Noamundi, India. Economic Geology, 103, 365–386.

Bhatia, M. R., and Crook, K. A. W., 1986. Trace element characteristics of graywackes and tectonic setting discrimination of sedimentary basins. Contributions to Mineralogy and Petrology, 92, 181-193.

Bhatia, M. R., 1983. Plate tectonics and geochemical composition of sandstones. Journal of Geology, 91, 611–627.

Bluck, B. J., 1971. Sedimentation in the meandering River Endrick. Scottish Journal of Geology, 7, 93-138.

Collinson, J. D., Bevins, R. E., and Clemmensen, L. B., 1989. Post-Glacial mass flow and associated deposits preserved in paleovalleys: the Late Precambrian Moreneso Formation, North Greenland. Medd.Gronland, Geoscience, 21, 3-26.

Cox, R., and Lowe, D. R., 1996. Quantification of the effects of secondary matrix on the analysis of sandstone composition, and a petrographic-chemical technique for retrieving original framework grain modes of altered sandstones. Journal of Sedimentary Research, 66, 548-558.

Dey, S., Topno, A., Liu, Y., Zong, K., 2017. Generation and evolution of Palaeoarchaean continental crust in the central part of the Singhbhum craton, eastern India. Precambrian Research, 298, 268-291.

Dickinson, W. R., 1985. Interpreting Provenance relations from Detrital Modes of Sandstones. *In*: Zuffa, G.G. (Ed.), Provenance of Arenites. Dordrecht. The Netherlands, D. Reidel, 333-361.

Dickinson, W. R., and Suczek, C. A., 1979. Plate tectonics and sandstone compositions. American Association of Petroleum Geology Bulletin, 63, 2164-2182.

Dickinson, W. R., Beard, L. S., Brakenridge, G. R., Erjavec, J. L., Ferguson, R. C., Inman, K. F., Knepp, R. A., Lindberg, F. A., and Ryberg, P. T., 1983. Provenance of North American Phanerozoic sandstones in relation to tectonic setting. Geological Society of America Bulletin, 94, 222-235.

Eriksson, K. A., 1978. Alluvial and destructive beach facies from the Archean Moodies Group, Barberton Mountain Land, South Africa and Swaziland. *In*: Miall, A.D. (Ed.), Fluvial Sedimentology. Memoir Canadian Society of Petroleum Geologists, 5, 287–312.

Fedo, C. M., and Cooper, J. D., 1990. Braided alluvial to marine transition: the basal Lower Cambrian Wood Canyon Formation, southern Marble Mountains, Mojave Desert, California. Journal of Sedimentary Petrology, 60, 220–234.

Fedo, C. M., Nesbitt, H. W., and Young, G. M., 1995. Unraveling the effects of potassium metasomatism in sedimentary rocks and paleosols, with implications for paleoweathering conditions and provenance. Geology, 23, 921–924.

Gray, D. I., and Benton, M. J., 1982. Multidirectional Paleocurrent as Indicators of Shelf Storm Beds. Cyclic and Event Stratification, 350-352.

Griffin, W. L., Wang, X., Jackson, S. E., Pearson, N. J., O'Reilly, S. Y., Xu, X., and Zhou, X., 2002. Zircon chemistry and magma mixing, SE China: In-situ analysis of Hf isotopes, Tonglu and Pingtan igneous complexes. Lithos, 61, 237–269.

Harnois, L., 1988. The CIW Index: A new Chemical Index of Weathering. Sedimentary Geology, 55, 319-322.

Heubeck, C., and Lowe, D. R., 1994. Depositional and tectonic setting of the Archean Moodies Group, Barberton Greenstone Belt, South Africa. Precambrian Research, 68, 257-290.

Krinsley, D. H., Tovey, N. K., 1978. Cathodoluminescence in quartz sand grains. *In:* Johari, O., (Ed.), Scanning Electron Microscopy. SEM Inc., AMF O'Hare, Illinois, 1, 887-894.

Mazumdar, R., Van Loon, A. J., Mallik, L., Reddy, S. M., Arima, M., Altermann, W., Eriksson, P. G., and De, S., 2012. Mesoarchaean-Palaeoproterozoic Stratigraphic record of the Singhbhum crustal province: a systhesis. Palaeoproterozoic of India. Geological Society, London, Special Publications, 365, 31–49.

Miall, A. D., 1978. Lithifacies types and vertical profile models of braided river deposits, a summary. *In*: A. D. Miall (Ed.), Fluvial Sedimentology. Memoir Canadian Society of Petroleum Geologist, 5, 597-604.

Misra, S., 2006. Precambrian Chronostratigraphic Growth of Singhbhum-Orissa Craton, Eastern Indian Shield: An Alternative Model. Journal of Geological Society of India, 67, 356-378.

Mueller, W. U., and Corcoran, P. L., 1998. Late-orogenic basins in the Archean Superior Province, Canada: characteristics and inferences. Sedimentary Geology, 120, 177–203.

Mukhopadhyay, J., Mishra, B., Chakrabarti, K., De, S., and Ghosh, G., 2015. Uraniferous paleoplacers of the Mesoarchean Mahagiri Quartzite, Singhbhum craton, India: Depositional controls, nature and source of >3.0 Ga detrital uraninites. Ore geology Review, 72, 1290-1306.

Mukhopadhyay, D., 2001. The Archaean nucleus of Singhbhum: the present state of knowledge. Gondwana Research, 4, 307–318.

Mukhopadhyay, J., Beukes, N. J., Armstrong, R. A., Zimmermann, U., Ghosh, G., and Medda, R. A., 2008. Dating the Oldest Greenstone in India: A 3.51-Ga Precise U-Pb SHRIMP Zircon Age for Dacitic Lava of the Southern Iron Ore Group, Singhbhum Craton, The Journal of Geology, 116, 449–461.

Mukhopadhyay, J., Crowley, Q., Ghosh, S., Ghosh, G., Chakrabarti, K., Mishra, B., Heron, K., and Bose, S., 2014. Oxygenation of the Archean atmosphere: New paleosol constraints from eastern India. Geology, 42, 923-926.

Mukhopadhyay, J., Ghosh, G., Beukes, N. J., Gutzer, J., 2007.Precambrian colluvial iron ore in the Singhbhum craton: implications for the origin age of BIF- hosted high grade iron ores and stratigraphy of the Iron Ore Group. Journal of the Geological Society of India, 70, 34-42.

Nemec, W., and Steel, R. J., 1984. Alluvial and coastal conglomerates: their significant features and some comments on gravelly mass-flow deposits. *In*: Koster, E. H., and Steel, R. J., (Ed.), Sedimentology of gravels and conglomerates. Memoir of Canadian Society of Petroleum Geologists, 10, 1-31.

Nesbitt, H. W., 2003. Petrogenesis of siliciclastic sediments and sedimentary rocks. *In:* Lentz, R. D., (Ed.) Geochemistry of Sediments and Sedimentary Rocks: Evolutionary considerations to mineral-deposit-forming environments. Geological Association of Canada, GEO Text, 4, 39–51.

Nesbitt, H. W., and Young, G. M., 1984. Prediction of some weathering trends of plutonic and volcanic rocks based on thermodynamic and kinetic considerations. Journal of Geology, 48, 1523-1534.

Nesbitt, H. W., and Young, G. M., 1989. Formation and Diagenesis of weathering profiles. The Journal of Geology, 97, 129-147.

Orton, G. J., and Reading, H. G., 1993. Variability of Deltaic processes in terms of sediment supply, with particular emphasis on grain size. Sedimentology, 40, 475-512.

Patchett, P. J., Kouvo, O., Hedge, C. E., Tastumoto, M., 1981. Evolution of continental crust and mantle heterogeneity: evidence from Hf isotopes. Contributions to Mineralogy and Petrology, 78, 279–297.

Roser, B. P., and Korsch, R. J., 1986. Determination of Tectonic setting of sandstone-mudstone suites using SiO_2 content and K_2O/Na_2O ratio. Journal of Geology, 94, 635-650.

Saha, A. K., 1994. Crustal evolution of Singhbhum–North Orissa, eastern India. Memoir of the Geological Society of India, 27, 1-341.

Seyedolali, A., Krinsley, D. H., Boggs S., JR., O'Hara, P. F., Dypvik, H., Goles, G. G., 1997. Provenance interpretation of quartz by scanning electron microscope-cathodoluminescence fabric analysis.Geology, 25, 787–790.

Tanner, L. H., and Hubert, J. F., 1991. Basalt breccias and conglomerates in the lower Jurassic McCoy Brook Formation, Fundy basin, Nova Scotia: differentiation of Talus and debris flow deposits. Journal of Sedimentary Petrology, 61, 15-27.

Taylor, S. R., and McLennan, S. M., 1985. The continental crust: its composition and evolution. Blackwell, 312 p.

Witts, D., Hall, R., Nicols, G., Morley, R., 2012. A new depositional and provenance model for the Tanjung Formation, Barito Basin, SE Kalimantan, Indonesia. Journal of Asian Earth Sciences, 56, 77-114.

FIGURES CAPTION

Figure. 1. Generalized geological map of the Singhbhum Craton(modified after Saha (1994).

Figure. 2. Geological map of the Keonjhar Quartzite from north of Keonjhar Town.

Figure. 3. Composite stratigraphic succession of the Keonjhar Quartzite. Note: two members classified within this formation: Asurkhol Member and Chamakpur Member.

Figure. 4. Field photographs of megascopic deformation structures close to major faults: in Keonjhar Quartzite (A) locally developed asymmetric fold and (B) strong fracture cleavage.

Figure. 5. Field photographs of different types of facies from Keonjhar Quartzite:(A) Matrix-supported cobble-to-pebble conglomerate facies (F1), (B) Clast-supported cobble-to-pebble conglomerate facies (F2), (C) Wavy bedded pebbly sandstone (F3), (D) Fine-chip pebble conglomerate (F4), (E) Coarse massive sandstone with pebble float facies (F5) and (F) Pebble lag facies (F6).

Figure. 6 Field photographs of different types of facies from Keonjhar Quartzite: .(A) Trough cross-stratified medium-grained sandstone facies (F7), (B) Plane-laminated medium-grained mature sandstone facies (F8) , (C) Wavy bedded medium-grained sandstone facies (F9), (D) Internal bedsets of cross-strata in wavy bedded structure of medium grained sandstone facies (F9).

Figure.7. Facies Associations from along down dip sections of the succession. Note facies associations of distal facies belts dominate towards west suggesting westerly paleoslope.

Figure. 8. Paleocurrent distribution pattern from trough cross-stratified sandstones of the Keonjhar Quartzite, Singhbhum Craton, Odisha..

Figure. 9. Grain-size distribution histogram pattern conglomerate facies (ten largest clasts measured from each bed). Note. enrichment of smaller fraction towards west.

Figure. 10. Schematic depositional model for the Keonjhar Quartzite.

Figure. 11. Depositional sequence and systems tract from Keonjhar Quartzite.

Figure.12.Optical and Scanning Electron micrographs of sandstones from Keonjhar Quartzite: (A) quartzarenite with sutured grain boundary in quartz framework population. (B) Quartzite fragment within pseudomatrix. (C) Recycled well rounded quartz grain with syntaxial broken overgrowth. (D) Secondary matrix distribution around quartz grain

Figure. 13. (A) Qt-F-L compositional plots (after Dickinson and Suczek, 1979) of arenites. Note samples cluster in cratonic interior to recycled orogen fields. (B) Qm-F-Lt compositional plots (after Dickinson et al., 1983; Dickinson, 1985) of arenites. Note all the samples cluster in

the quartzose recycled to cratonic interior origin. (C) Qm-P-K compositional plots (after Dickinson and Suczek, 1979) of arenites. Note all the samples cluster in the stable continental block provenance.

Figure. 14. SEM CL images of images of plutonic quartz from the Keonjhar Quartzite. (A) plutonic quartz with low luminescent and thin hairline healed fracture. (Note Healed fracture). (B) plutonic quartz where healed fracture filled by secondary fluid inclusion (foreign material or trace element like Li, Al, Ti) that produce dark streak and patches. (Note Healed fractures are filled by foreign material and produce dark patches). (C) Dark streak and patches in plutonic quartz grain. (D) Fractures are sparsely distributed and widely spaced as more than one set of lines. Note the fractures intersect at constant angles.

Figure.15. SEM CL images of low to medium grade metamorphic quartz from the Keonjhar Quartzite. (A) Inhomogeneous and patchy mottled luminosity in medium grade metamorphic quartz grain. (B) CL patterns of image of low grade metamorphic dominated detrital quartz population.(C) Medium-to-high grade deformed quartz grain produce brittle fracture. (D) Cathodoluminescence (CL) image of high-grade (bright luminosity) deformed quartz grain.

Figure.16. Plots of major oxide composition from the Keonjhar Quartzite in different tectonic setting discrimination diagrams (after Roser and Korsch, 1986). (A) Plot in diagram using (Fe2O3 + MgO) versus (Al2O3/SiO2). Note that the all samples-plot very close to the fields of passive continental margins. (B) Plot in diagram using (Fe2O3 + MgO) versus TiO2 content. Note that majority of the samples plot within and very close to the passive margin field. (C) Plot in SiO2 versus K2O/Na2O Note that all of the samples Keonjhar Quartzite plot in the passive margin field. (D) Plot in SiO_2/Al_2O_3 versus K_2O/Na_2O diagram from major oxide data from the Mesoarchean sandstone in different tectonic setting discrimination diagrams (after Roser and Korsch, 1986). Note that all of the samples Keonjhar Quartzite plot in the passive margin field.

Figure. 17. Plots of major oxide data in A-CN-K diagram (after Nesbitt and Young 1984). Note that the plots for the QPC, sandstone and mudstone samples show a distinct linear weathering trend parallel to the A-K side of the diagram.

Figure. 18. (A) La–Th–Sc discriminatory plot (after Bhatia andCrook, 1986) for Mesoarchean Keonjhar Quartzite. Note that most of the samples plot within and close to the boundary of the fields of passive and active continental margin settings and three samples each from this formation plot in the field of oceanic island arc. (B) Th–Sc–Zr/10 discriminatory plot (after Bhatia and Crook, 1986) of Mesoarchean siliciclastics samples from the Keonjhar basin. Note that most of the siliciclastic samples plot within and close to the fields of both active and

passive continental margins and three samples of this formation plot in the field of oceanic island arc.

Figure. 19. Spider plots of trace element composition normalized with Archean upper crust (AUC) from the Mesoarchean Keonjhar Quartzite. (A)Trace elements normalized with Archean upper crust (AUC) with respect to sandstone. (B) Trace elements normalized with Archean upper crust (AUC) with respect to QPC.

Figure. 20. Plots of Rare earth element (REE) composition normalized with Archean upper crust (AUC) from the Keonjhar Quartzite:. (A) REE Compositions of sandstones. (B) REE compositions from QPCs (Quartz Pebble Conglomerate) within Keonjhar Quartzite.

Figure. 21. (A) $€^{Hf(t)}$ versus $^{207}Pb/^{206}Pb$ Age(Ma) diagram showing results for detrital zircon from the Mesoarchean Keonjhar Quartzite (<3 Ga depositional age). (B) Detrital zircon TDM model age vs $^{207}Pb/^{206}Pb$ Age (Ma) diagram. Note the Hf model age is much older than the crystallisation age. (C) Detrital zircon $^{176}Hf/^{177}Hf$ versus $^{207}Pb/^{206}Pb$ Age (Ma) diagram showing that 'Juvenile continental crust' was dominant component in the granitoids at source of the sediments.

Figure. 22. Schematic diagram of accretionary orogen juvenile crust emplacement.

Figure. 23. (A)SEM- images of Brannerite grain from QPC samples of Keonjhar Quartzite. (B) SEM- EDS analysis of uraniferous leucoxene grain from QPC samples of Keonjhar Quartzite. (C) SEM- EDS analysis of Uraniferous leucoxene grain from QPC samples of Keonjhar Quartzite.

Figure. 24. Keonjhar QPC variations in spider plot normalised with respect to sandstones: A. major oxide Note: variable enrichment in Fe_2O_3, Na_2O, TiO_2 and MnO and depletion in MgO, K_2O and P_2O_5. B. trace element compositions normalised with respect to sandstone. Note Enrichment in Cr, Ni, Th, U, Sr and Pb in QPC and depletion in Co, Rb, Cs and Ba. C. REE pattern. Note enrichment in LREE in QPC and retention of negative Eu-anomaly.

Figure. 25. Plots of QPC major oxide data from the Keonjhar Quartzite (A) Major oxide normalized diagram with Singhbhum Granite phase I. (B) Major oxide normalized diagram with Singhbhum Granite phase II. (C)Major oxide normalized diagram with Singhbhum Granite phase III. (D)Major oxide normalized diagram with Singhbhum Granite (mean of all phases).

Figure. 26. Plots of QPC trace elements data from the Keonjhar Quartzite. (A) normalized with Singhbhum Granite phase I. (B) normalized diagram with Singhbhum Granite phase II. (C) normalized diagram with Singhbhum Granite phase III. (D) normalized diagram with Singhbhum Granite phase mean (mean of all phases)

Figure. 27. Plots of REE from the Keonjhar Quartzite (A) normalized diagram with Singhbhum Granite phase I. (B) normalized diagram with Singhbhum Granite phase II. (C) normalized diagram with Singhbhum Granite phase III. (D) normalized diagram with Singhbhum Granite (mean of all phases).

Figure. 28. SEM- EDS images and analyses of corona texture (rutile in the core of texture and brannerite in the rim) from Pronto Reaction.

Figure. 29. Matrix correlation diagram U-Th correlation with major oxides.

Figure. 30. Matrix correlation diagram U-Th correlation with trace elements.

Figure. 31. Matrix correlation diagram U-Th correlation with rare Earth elements.

Figure. 32. (A) Field photograph of lensoid iron ore conglomerate bodies mined out from Chamakpur Member. (B) Field photograph of iron ore conglomerate with clasts of hard iron ore (dark steel gray) and BIF (reddish) in Chamakpur Member. Note well rounded hard iron ore clast (near the left upper corner coin scale).

Figure. 33. BSE-SEM images of ore texture from clast of iron ore from iron ore bearing conglomerates (A) Anhedral and microplaty hematite. (B) Martite distribution surrounded by microplaty hematite.

Figure. 34. Detrital zircons LA-ICPMS U-Pb age ranging from 3.0–3.3 Ga (considered those zircons with <5% discordance limit) from sandstone clasts in iron ore conglomerate and overlying sandstone beds of Keonjhar Quartzite.

TABLE CAPTION

Table: 1 Proposed lithostratigraphic classification of Keonjhar Quartzite, Singhbhum craton, Odisha.

Table: 2. Salent Characteristics of lithofacies in the Keonjhar Quartzite.